Winter 2022

INVESTIGATING THE ROLE OF PALMITOYL ACYLTRANSFERASE 14 IN PREVENTING EARLY DEATH IN ARABIDOPSIS THALIANA

Robert Elliott
University of New Hampshire, Durham

INVESTIGATING THE ROLE OF PALMITOYL ACYLTRANSFERASE 14 IN PREVENTING EARLY DEATH IN *ARABIDOPSIS THALIANA*

BY

ROBERT ELLIOTT

B.S, University of New England, 2018

THESIS

Submitted to the University of New Hampshire

in Partial Fulfillment of

the Requirements for the Degree of

Master of Science

in

Biochemistry

December 2022

This thesis has been examined and approved in partial fulfillment of the requirements for the degree of Master's in Biochemistry by:

Dr. Estelle Hrabak, Thesis Director, (Molecular, Cellular, & Biomedical Sciences)

Dr. Krisztina Varga, Associate Professor, (Molecular, Cellular, & Biomedical Sciences)

Dr. Kelley Thomas, Professor, (Molecular, Cellular, & Biomedical Sciences)

On November 17th, 2022

Approval signatures are on file with the University of New Hampshire Graduate School

ACKNOWLEDGEMENTS

I'd like to thank the many plants that were sacrificed, my fiancée Audrie, my mentor Dr. Estelle Hrabak, and my committee members, Dr. Krisztina Varga and Dr. Kelley Thomas. Further, I'd like to thank Dr. Anthony Westbrook, Dr. Jeff Halpern, and David Moore for materials and programming education.

Table of Contents

PAGE

List of Tables

List of Figures

ABSTRACT

Palmitoylation is a reversible post-translational modification that affects the location, activity, and stability of proteins. *Arabidopsis thaliana* contains 24 genes for palmitoyl acyltransferases (PATs), the enzymes that catalyze palmitoylation. Loss of PAT14 activity results in early senescence and diminished plant size when plants are grown on a standard peat/perlite mixture in pots and watered with a commercial fertilizer, but this phenotype is not observed when plants are grown on agar plates containing a different nutrient solution. Here we investigate the roles of the peat/perlite growth medium and the presence of microbes in the environment in phenotype development. The *pat14-1* early senescence phenotype was partially rescued by supplementing commercial fertilizer with uric acid. XDH1 (xanthine dehydrogenase) produces uric acid and is also predicted to be palmitoylated. An *xdh1* mutant has a phenotype similar to the *pat14* mutant, raising the possibility that XDH1 is a palmitoylation substrate of PAT14. Immunodetection of XDH1 showed that its subcellular localization was not affected in a *pat14* background. However, there appeared to be a greater quantity of XDH1 in the cytosol of *pat14* mutants, indicating that XDH1 expression or stability is altered in the absence of PAT14.

INTRODUCTION

Palmitoylation

Regulation of protein activity is fundamental to maintaining cellular homeostasis. Methods to regulate protein activity include modification of proteins by phosphorylation, glycosylation, methylation, or lipidation[1]. This research focuses on one type of lipidation called palmitoylation.

Palmitoylation, a type of protein acylation, is the covalent attachment of the saturated 16-carbon fatty acid, palmitate, to a protein[2]. Palmitoylation occurs on solvent-exposed cysteines and is catalyzed by two families of integral membrane enzymes - the palmitoyl acyltransferases (PATs) and the membrane-bound O-acyltransferases (MBOATs)[3,4]. PATs catalyze S-palmitoylation, which is the attachment of palmitate to a non-terminal cysteine residue via a thioester bond (Figure 1A). MBOATs catalyze N-palmitoylation or the attachment of palmitate to an amido-terminal cysteine via an amide bond (Figure 1B)[5]. S-palmitoylation is more common than N-palmitoylation. Unique among lipid modifications, S-palmitoylation is reversible, allowing for spatio-temporal control of protein activity[2]. Depalmitoylation is controlled by the acyl protein thioesterase family of enzymes (APT) [6,7].

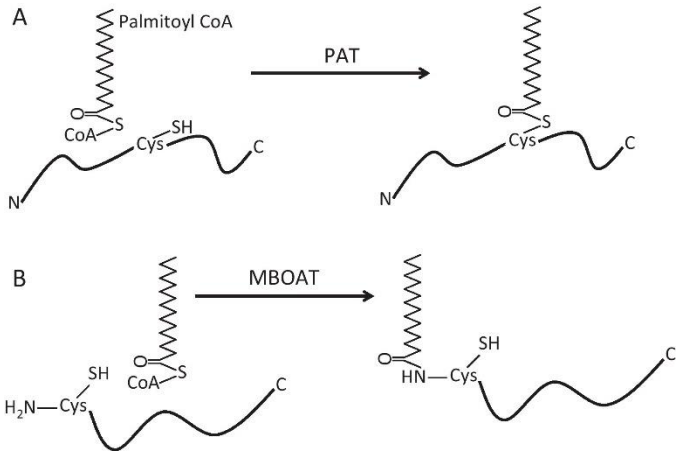

Figure 1. Biochemistry of palmitoylation. A) In S-palmitoylation, palmitic acid is added to proteins at cysteine residues via a thioester bond by palmitoyl acyltransferases (PATs). B) In N-palmitoylation, palmitic acid is added to N-terminal cysteines via an amide bond by members of the membrane-bound O-acyltransferase (MBOAT) family. Both reactions use palmitoyl-CoA as the lipid substrate. Modified from Young et al. (2012)[8].

Palmitoylation has a range of impacts on substrate proteins including modulation of enzyme activity or stability, regulation of protein-protein interactions, and alteration of subcellular localization[9–12]. Increased transmembrane protein stability caused by palmitoylation appears to arise by preventing recognition by the proteasome pathway[12]. Protein-protein interactions can be dependent on or inhibited by palmitoylation, while palmitoylation-induced changes in subcellular localization can regulate entry of proteins into lipid raft domains or compel a cytosolic protein to become membrane-associated[9,13,14].

No conserved S-palmitoylation motif has been identified. Palmitoylation often occurs subsequent to myristoylation or prenylation, although palmitoylation can occur independent of myristoylation or prenylation as well[4,14–16]. Myristoylation, the addition of 14-carbon saturated myristic acid to a protein, requires an amino acid motif beginning with an N-terminal glycine. Commonly this glycine is revealed after the typical proteolytic cleavage of the N-terminal methionine from a nascent protein but internal cleavage that creates an N-terminal glycine has also been reported[5,15]. Prenylation, the addition of a farnesyl or geranylgeranyl group, occurs at a carboxy-terminal *CaaX*, *CXC*, or a *CC* motif, where *C* is cysteine, *a* is generally an aliphatic amino acid, and *X* is a specific amino acid that determines whether the attached moiety will be a farnesyl or a geranylgeranyl group[2]. Both myristoylation and prenylation promote transient interaction of the lipidated protein with cellular membranes and thus brings the protein into proximity of membrane-localized PAT enzymes. The kinetic bilayer trapping hypothesis states that dual lipidation (e.g., both myristoylation and palmitoylation) creates a stable, long-term membrane association, significantly stronger than myristoylation alone[16].

Palmitoyl Acyltransferases

Palmitoyl acyltransferases (PATs) are integral membrane proteins characterized by 4 to 6 transmembrane domains that contain a distinct DHHC (Asp-His-His-Cys) sequence motif embedded in a Cysteine-Rich Domain (DHHC-CRD)[17]. The cysteine in the DHHC motif is involved in both auto-palmitoylation and substrate palmitoylation[3]. The DHHC-CRD is almost invariably found on a cytoplasmic loop immediately preceding the third transmembrane domain (TMD)[17]. The proximity of the active site to a TMD indicates that PAT substrates are likely already membrane associated, whether because of either a previous lipidation event or the presence of a protein domain with an inherent membrane affinity like the polybasic region (PBR) found in K-Ras[18]. First identified in *Saccharomyces cerevisiae* (baker's yeast) in 2002, PATs are found in eukaryotes, but not archaea or bacteria[3]. Most eukaryotes with sequenced genomes have multiple *PAT* genes, indicating diversification of roles for these enzymes [17,19,20] (**Table 1**).

The exact nature of the S-palmitoylation reaction mechanism remains an open question. Current evidence suggests S-palmitoylation proceeds via a two-step process requiring the DHHC motif[21–23]. The first histidine is polarized by aspartate and extracts a proton from cysteine, creating a thiolate nucleophile. The cysteine thiolate then attacks the carbonyl carbon of a fatty acyl-CoA thioester, releasing CoA and creating an autoacylated PAT. Next, it is proposed that the protonated histidine activates the carbonyl of the thioesterified cysteine in the DHHC motif, causing the cysteine present on the substrate protein to attack that carbonyl carbon. The palmitate is then transferred to the substrate's cysteine, regenerating the DHHC region for further catalysis[21–23].

Table 1. Number of *PAT* genes in various eukaryotes. Collected from SwissPalm[24] .

Organism	Number of *PAT* genes
Saccharomyces cerevisiae	7
Bos taurus	7
Neospora caninum	17
Toxoplasma gondii	18
Drosophila melanogaster	20
Homo sapiens	23
Arabidopsis thaliana	24
Mus musculus	25

Mutations that change amino acids in the DHHC motif have cast doubt on individual steps of this process. Mutation of cysteine to arginine did not impact the activity state of the enzyme, implying that enzyme autoacylation may not be required[22]. Further, autoacylated states have not been detected for several mammalian PATs despite the perceived mechanistic need[25]. Finally, DHHC13 in mice is functional but contains a DQHC motif and mutation of glutamine to histidine did not impact the catalytic ability of the enzyme, while mutation of the first histidine to glutamine in the closely-related DHHC17 enzyme abolished all catalytic activity[25]. In contrast, a similar histidine to glutamine mutation in a yeast PAT retained some activity[26].

All PAT-substrate interactions are likely bolstered by protein-ligand interactions, since this would provide a mechanism for fine-tuning substrate specificity, but only a few examples are known to date. Human PATs zDHHC5, zDHHC8, and zDHHC14 all contain a binding site for PDZ (PSD-95/discs large/ZO-1) domains[27,28]. The PDZ binding domain is required for zDHHC5 and zDHHC8 to palmitoylate glutamate receptor-interacting protein 1 (GRIP1), for zDHHC8 to palmitoylate protein interacting with C-kinase 1 (PICK1), and for zDHHC14 to palmitoylate PSD93 (postsynaptic density 93)[29–31].

Every PAT is membrane-localized, but any given PAT might be confined to one specific membrane or distributed among several membranes throughout the cell. For example, a variety of localization types are demonstrated by the PAT family in Arabidopsis[17]. Many Arabidopsis PATs are found only in the plasma membrane, while others are detected in both the plasma membrane as well as on transport vesicles (**Table 2**). PAT localization determines where its substrates are initially palmitoylated and first become membrane anchored. However, post-palmitoylation, palmitoylated proteins may be trafficked to other membrane locations via vesicle-mediated transport[32,33].

Table 2. Subcellular localizations of PAT proteins in *Arabidopsis thaliana*. Adapted from Batistic et al[17].

Localization	Arabidopsis PAT
ER (and vesicles)	AtPAT03
	AtPAT15
	AtPAT17
	AtPAT18
Vesicles (Golgi)	AtPAT10
	AtPAT16
Vesicles (Golgi and non-Golgi)	AtPAT14
	AtPAT24
Vesicles (non-Golgi)	AtPAT01
	AtPAT02
PM and vesicles	AtPAT13
	AtPAT20
	AtPAT22
PM	AtPAT04
	AtPAT05
	AtPAT06
	AtPAT07
	AtPAT08
	AtPAT09
	AtPAT12
	AtPAT19
	AtPAT21
Tonoplast	AtPAT10
	AtPAT11

Effect of Palmitoylation on Cytosolic Proteins

The impact of palmitoylation depends on the protein in question. For cytosolic proteins, palmitoylation can serve as an "on-off" switch for membrane association, including association with lipid rafts[34,35]. For example, in mammals, Ras proteins are critical regulators of cell growth and differentiation[36]. All three Ras isoforms, N-Ras, K-Ras, and H-Ras, have a farnesylation site at their carboxyl terminus[22]. N-Ras and H-Ras are farnesylated in the cytoplasm leading them to interact with ER or Golgi membranes, respectively, where their palmitoyl transferases reside, leading to palmitoylation[37–39]. The increased hydrophobicity caused by dual lipidation initially anchors Ras to the membrane where palmitoylation occurs. K-Ras is distinct from the other two isoforms in that palmitoylation is not necessarily required for plasma membrane targeting; instead K-Ras uses a polybasic region (PBR) of eight lysine residues that provides a weak affinity for the plasma membrane for its initial membrane binding and then subsequent palmitoylation dramatically improves the binding affinity[18].

Lipidated N-Ras or H-Ras proteins travel to the plasma membrane in vesicles via the secretory pathway because Ras functions at the cell surface[35]. Ras can be depalmitoylated by an APT and dissociate from the cell surface, returning to the Golgi complex or ER via nonvesicular transport[39]. Ras is a good example of how palmitoylation of cytosolic proteins functions in protein localization and as a regulated "on-off" switch when partnered with an APT.

Effect of Palmitoylation of Integral Membrane Proteins

In contrast to cytosolic proteins, integral membrane proteins are inherently membrane associated and so palmitoylation does not result in membrane anchoring but can affect activity, protein-protein association, localization, or entrance to lipid rafts[40–44]. The palmitoylation site on integral membrane proteins is usually within 10 amino acids of a transmembrane domain to enable insertion of the palmitate moiety into the membrane.

Lipid rafts are sub-regions within a membrane that are enriched in sphingolipids and contain specific protein complexes[45]. Palmitoylation of integral membrane proteins can drive lipid raft association. For example, palmitoylation of the human integrin α6β4 receptor is required for entry into lipid rafts, subsequent association with members of the palmitoylated Src family kinases (SFK), and transmission of mitogenic signals[46]. In rare cases, palmitoylation prevents lipid raft association as in the case of the anthrax toxin receptor protein TEM8 leading to ubiquitination and degradation of TEM8[47].

Palmitoylation Prediction

Predicting protein modifications through computational methods has been a long-sought goal in biochemistry. Searching proteomic databases for identifiable sequence motifs indicative of an interaction is less energy- and funding-intensive than testing protein sets *in vitro*. As more protein modifications are confirmed, the training datasets for computational methods have increased in size and improved in their ability to identify consensus sequences. For example, programs for the identification *O*-GlcNAcylation sites have reliably determined a

P-P-V-[ST]-T-A consensus sequence and exceptions to the rule continue to be identified and used to improve the programs[48]. Other programs, such as PhosphoPredict, are able to predict phosphorylation sites and the accompanying protein-kinase interaction[49].

A significant roadblock in palmitoylation prediction is the lack of identifiable conserved amino acid motif(s) apart from the required cysteine. A number of tools have been developed, and continue to be improved, to predict palmitoylation including CSS-Palm, GPS-Palm, WAP-Palm, and PalmPred[50–53]. However, these programs currently show limited accuracy when compared to experimental results. In particular, CSS-PALM 4.0 only identified 25% of experimentally identified palmitoylated protein sites in *A. thaliana*[54]. Currently, known and validated palmitoylated proteins are organized in SwissPalm, an online database of palmitoylated proteins[55].

Arabidopsis thaliana as a Plant Model Organism

Arabidopsis thaliana is a small flowering plant with a rapid life cycle of 8-10 weeks under long-day conditions[56]. Its small size, ease of growth, and abundant seed production make it a widely used model organism for plant research. *A. thaliana* has 5 chromosomes, a total genome size of ~135 Mb, and 24 palmitoyl acyltransferase genes spread across the five chromosomes that are all expressed[17]. The PAT proteins vary in size from 254 to 718 amino acids[17].

Of an estimated 14,430 proteins in the *A. thaliana* proteome, 2643 are believed to be palmitoylated based on experimental data[54,57]. If one assumes that palmitoylation is non-redundant and that the work of palmitoylating those 2643 substrates is evenly distributed among

the 24 PATs, then each PAT might palmitoylate more than 100 proteins. That number could be higher if multiple PATs act on the same substrate.

At present, fewer than two dozen of the predicted palmitoylated substrates have been connected to a specific PAT[55]. For example, AtPAT5 and AtPAT9 have both been shown to palmitoylate the plant immune receptor P2K1 to restrict plant immune response[58]. PAT10 palmitoylates several calcineurin B-like proteins (CBL2, CBL3, CBL6, and CBL10) that maintain cellular magnesium and NaCl homeostasis[59,60]. PAT4 mediates root hair growth by palmitoylating Rho of Plants 2 (ROP2) to mediate its membrane association[61].

PAT14 in Arabidopsis

Two *A. thaliana* PATs, PAT13 and PAT14, share 66% amino acid identity across 302 and 307 amino acids, respectively[17]. Individual knock-out mutations of the *pat13* or *pat14* genes show a moderate early senescence phenotype with plants beginning to yellow as early as 4-5 weeks of age while a double knock-out of both *pat13* and *pat14* showed senescence as early as 3 weeks of age[62]. Additionally, *pat14* mutants are smaller than wildtype plants (**Figure 2**) but retain a similar cell count, indicating that the diminished size does not originate from a reduced number of cells but rather that the cells themselves are smaller than cells in wildtype plants[63]. Flowering time is not affected and both double mutant and single mutant plants are able to produce seeds[62]. Due to the high sequence similarity between PAT13 and PAT14, and the additive impact of the double knockout, it seems likely that PAT13 and PAT14 share some substrates, although none have been identified. PAT14 is the focus of this work.

Figure 2. Phenotype of the *pat14-1* mutant. Wildtype (left) and *pat14-1* mutant (right) *Arabidopsis thaliana* plants were grown in peat-perlite potting mix for four weeks under long-day conditions at 21 ºC and fertilized with MiracleGro. (Photo courtesy of J. McLarney & E. Hrabak)

PAT14 is ubiquitously expressed throughout the Arabidopsis lifecycle with a moderate increase in older leaves and localizes to the trans-Golgi network[62–65]. Since proteins that proceed through the Golgi network are usually destined for other cellular locations, the localization of PAT14 does not readily help narrow the list of possible protein targets.

The PAT14 null mutant used here, *pat14-1*, was generated via *Agrobacterium tumefaciens* T-DNA insertion near the start codon of the *PAT14* gene[66]. *pat14-1* mutants accumulate hydrogen peroxide (H_2O_2) and salicylic acid (SA), both of which are positive regulators of senescence and pathogen defense[62,63]. At low concentrations, H_2O_2 functions as a signaling molecule involved in a variety of plant processes ranging from growth to germination to senescence; however, higher concentrations can cause oxidative damage to cells, so catalase enzymes are produced to convert H_2O_2 to water and oxygen[67]. Both SA biosynthetic pathway genes and SA-sensitive signaling proteins are strongly upregulated in *pat14-1* plants, showing that the plant is producing both more SA and more SA-sensitive receptors. Blocking SA signaling or depleting SA levels partially rescue *pat14-1* early senescence but does not extend the lifespan of the plant[63,68].

Additionally, *pat14-1* plants show strongly upregulated expression of defense response genes, such as the Pathogenesis-Related 1 gene (*PR1*)[63]. Up-regulation of defense-related genes during senescence does not require presence of a pathogen or elevated levels of SA[53]. That 'defense-related' genes can be expressed in the absence of any pathogens and during senescence, drives home the important idea that proteins and macromolecules are not inherently restricted to one biological trait or phenomenon. Pleiotropy can make discerning the mechanisms and downstream effects of mutations difficult to tease out.

Goals of This Work

The objective of this work was to identify substrates of PAT14 palmitoylation and employed three approaches. The first approach was a continuation of work done by previous graduate students that showed that growth on agar plates prevented the development of the *pat14-1* early senescence phenotype. Components of the plant growth medium, as well as the sterility of the environment, were modified to look for an effect on phenotype development. The second approach used a novel bioinformatic-based method to identify proteins with phenotypes similar to *pat14-1*. A custom script was written to identify possible protein palmitoylation targets in the predicted Arabidopsis proteome. Third, published literature was searched for other plant mutants with similar phenotypes to *pat14-1* that might indicate a possible interaction in the same pathway. Xanthine Dehydrogenase 1 (XDH1) was identified as a possible target of PAT14 because XDH1 is known to be palmitoylated and has a knock-out phenotype similar to the phenotype of *pat14-1*.

METHODS

Arabidopsis Genes and Genotypes

The wildtype ecotype of *Arabidopsis thaliana* used in this study was Columbia-0 or Col-0. The Arabidopsis PAT14 protein is encoded by a gene on chromosome 3 (At3g60800). The PAT14 mutant used here was created by insertion of a T-DNA near the start codon (SALK_026159)[66] and is designated *pat14-1*[62].

Bioinformatics Prediction

The latest proteome release for Arabidopsis (Araport11) was downloaded from The Arabidopsis Information Resource (TAIR)[69,70]. Biological Process (BP) Gene Ontology (GO) terms were retrieved from TAIR (ATH_GO_GOSLIM). GPS-PALM (http://gpspalm.biocuckoo.cn/) was used to identify proteins predicted to have palmitoylation sites[52]. Code and notes for my custom script for palmitoylation targets are available on Github at https://github.com/robelliott4996/PAT14

Surface Sterilization of Seeds

Seeds (40 mg) were immersed in 14 mL 70% (v/v) ethanol containing 150 µL of 10% (v/v) Triton X-100 for 5 minutes with occasional agitation of the container. After decanting the liquid, seeds were washed with 14 mL 100% ethanol containing 150 µL of 10% Triton X-100 for

5 minutes with occasional agitation of the container. After decanting the liquid, seeds were rinsed with 100% ethanol for 5 minutes before decanting the ethanol and drying the seeds completely in a laminar flow hood.

Growth of Plants in Peat/Perlite

Seeds were surface-sown in 2.25" square pots in a 1:1 (v:v) mixture of PRO-MIX BK45-V peat/bark mix (BFG Supply Co, Burton, OH) and graded horticulture perlite (Whittemore, Inc., Lawrence, MA). Pots were placed in 27 cm x 53.5 cm flats at 21°C in a walk-in growth room (Controlled Environments Inc., Pembina, ND). Photoperiod was 16 hours at 100 µmol m^{-2} sec^{-1} from fluorescent lights. When an experiment used different genotypes, pots were randomly distributed in the flat to control for variations in local conditions within the growth room. Plants were bottom-watered as needed with tap water containing added nutrients; nutrient composition depended on the experiment. Nutrient sources were commercial fertilizer (Scotts MiracleGro, Prod# 3000992; 1X = one small scoop per gallon) or 0.5X Murashige-Skoog (MS) containing Gamborg's vitamins (MS) (Caisson, Prod# MSP06), pH adjusted to 5.7. In some experiments, these nutrients were supplemented with 100 µM uric acid.

To grow plants in a microbe-free environment, Magenta boxes half-filled with sterilized peat/perlite (1:1, v:v) mixture and moistened with water were autoclaved. Surface-sterilized seeds were sown on the surface of the mixture. Boxes were placed in a growth room at 21°C with a 16-hour photoperiod. Ten days after germination, plants were thinned to one plant per box using aseptic technique. Plants were watered once a week with autoclaved 1X MiracleGro. At 6 weeks of age, plant green mass was harvested and weighed.

Growth of Plants on Plates

300 mL of dry peat/perlite mixture (1:1; v:v) and 0.6% Phytoblend (Caisson Laboratories, PTC001) was added to 500 mL DI water. The mixture was autoclaved and cooled to ~60 °C. 0.25 g of MiracleGro fertilizer was dissolved in 50 mL distilled water and filter sterilized (0.2 µm) prior to adding the fertilizer to the autoclaved peat/perlite/Phytoblend mixture. 50 mL of the mixture was poured into 100 cm^2 plates marked with a 6 x 6 grid (FisherScientific, Cat. No. FB0875711A) and solidified. One-third of the gel (a 2 x 6 grid section) was removed with an autoclaved razor blade starting from one edge of the plate. Gel removal created a "shelf" where multiple surface-sterilized seeds were placed using a sterile pipette tip. Plates were oriented vertically and placed in a walk-in growth room at 21°C with a 16-hour photoperiod at 100 µmol m^{-2} sec^{-1} from fluorescent lights. Plates were sealed with micropore tape (3M Company) to minimize water evaporation. At 10 days after germination, seedlings were thinned to 6 per plate. After thinning, all plates contained three seedlings of one genotype on half of the plate and three seedlings of a different genotype on the other half of the plate. Plates were returned to the growth room for the duration of the experiment.

Image Analysis of Senescent Leaves

Digital images of plants grown in pots were analyzed using ImageJ[71] to measure yellow versus green leaf area as a quantitative measure of chlorosis and senescence. Colored pixels were segregated on the basis of Hue with values from 0-40 corresponding to yellow leaf sections and values of 41-255 corresponding to green leaf sections.

Isolation and Quantification of Cytosolic and Membrane Proteins

Plant material was blotted dry, weighed, flash frozen in liquid nitrogen, and pulverized via mortar and pestle. Pulverized plant tissue was resuspended in Isolation buffer (50 mM Tris-HCl, pH 7.4, 150 mM NaCl, 5 mM EDTA, and 5 µL of plant protease inhibitor cocktail [Sigma-Aldrich, St. Louis, MO, Cat. No. P9599] per gram tissue). The suspension was filtered through MiraCloth (Calbiochem, Cat# 475855) to remove cell walls and large debris, then centrifuged at 5,000 x g for 10 minutes at 4°C to pellet intact organelles and small particulates. Supernatant containing soluble proteins and microsomes was collected and ultracentrifuged at 125,000 x g for 1 hour. The supernatant after ultracentrifugation contained cytosolic proteins and very small vesicles and was stored at -80ºC. The pellet, which contained membranes and membrane-associated proteins, was resuspended in 300 µL of Isolation buffer followed by homogenization in a dounce homogenizer. The membrane sample was stored at -80ºC. The volumes of both the supernatant and the resuspended pellet were noted to facilitate loading of proportional amounts of each sample on SDS-polyacrylamide gels. Protein concentration was determined using a Bradford protein assay (Bio-Rad, Cat# 500-0006) using BSA as the standard.

Protein Electrophoresis and Immunodetection

Protein samples were diluted with 4x Laemmli loading buffer (125 mM Tris-HCl, pH 6.8, 4% (w/v) SDS, 20% (v/v) glycerol, 5% β-mercaptoethanol) and heated at 70°C for ten minutes. Proportional volumes of cytosolic sample and membrane sample were resolved on a 10% SDS-polyacrylamide gel at 120 V for ~1 h. After electrophoresis, proteins were transferred to

Immobilon (Millipore, Billerica, MA) polyvinylidene difluoride membrane using transfer buffer (25 mM Tris, 192 mM glycine, pH 8.3, 20% methanol (v/v)) for 1 hour, then dried between two sheets of blotting paper.

For immunodetection, the membrane was rewetted in 100% methanol and blocked overnight in blocking buffer (20 mM Tris-HCl, pH 7.6, 137 NaCl, 0.05% (v/v) Tween-20, 5% (w/v) non-fat dry milk) at 4°C. After blocking, the membrane was incubated with primary antibody in blocking buffer. After washing three times for 5 minutes each with wash buffer (20 mM Tris-HCl, pH 7.6, 137 NaCl, 0.05% (v/v) Tween-20, 0.5% (w/v) non-fat dry milk), the blot was incubated with goat anti-rabbit secondary antibody conjugated to horseradish peroxidase (1:20,000, Pierce ImmunoPure Cat. No. 31462). After three washes with wash buffer as described above, the blot was saturated with SuperSignal™ West Dura Extended Duration Substrate (Thermo Scientific Cat. No. 34075) or SuperSignal™ West Femto Maximum Sensitivity Substrate (Thermo Scientific Cat. No. 34095) following manufacturer's instructions, exposed to X-ray film, and the film was developed with standard photo-processing chemicals. Primary antibodies were: polyclonal anti-xanthine dehydrogenase 1 (XDH) (1:1000, PhytoAB Inc. Cat# PHY1013S) and VM23 (1:3000, from M. Maeshima, Hokkaido University, Japan).

To perform another immunodetection on the same membrane, antibodies were removed with stripping buffer (62.5 mM Tris-HCl, pH 6.8, 2% (v/v) SDS, and 100 mM β-mercaptoethanol) at 50°C for 30 min, agitating every 10 minutes. The blot was then rinsed twice with wash buffer, followed by reblocking before incubating with other antibodies.

RESULTS

Role of Growth Medium Components in *pat14-1* Early Senescence

An early senescence phenotype for the *pat14-1* mutant has been described previously[62,63,68]. Although precise growth conditions were not provided, the figures in these publications either clearly show plants growing in pots or the plants have the appearance of being grown in pots, indicating that growth in potting medium is correlated with phenotype development. The Hrabak lab has replicated this published phenotype innumerable times when growing the *pat14-1* mutant on peat/perlite growth medium and watering with commercial fertilizer (MiracleGro)[65,72]. Wildtype plants look normal under these conditions (**Figure 2**).

Unexpectedly other experiments in the Hrabak lab showed that *pat14-1* plants grown under sterile conditions on agar plates containing a medium formulated for plant tissue culture (Murashige-Skoog with Gamborg vitamins) showed no early senescence phenotype (J. McLarney, personal communication). There are many differences between the two growth conditions: nutrient source (MiracleGro vs tissue culture medium), sterile environment, type of solid support (peat/perlite vs. agar), etc. To evaluate if presence of peat, perlite, and MiracleGro were correlated with development of the *pat14-1* senescence phenotype, both wildtype and *pat14-1* seeds were germinated and grown for four weeks under long day conditions on agar plates containing peat/perlite and MiracleGro solidified with Phytoblend agar. The *pat14-1* plants were visually indistinguishable from the wildtype plants under these conditions, indicating that the mutant phenotype was not produced under these conditions (**Figure 3**).

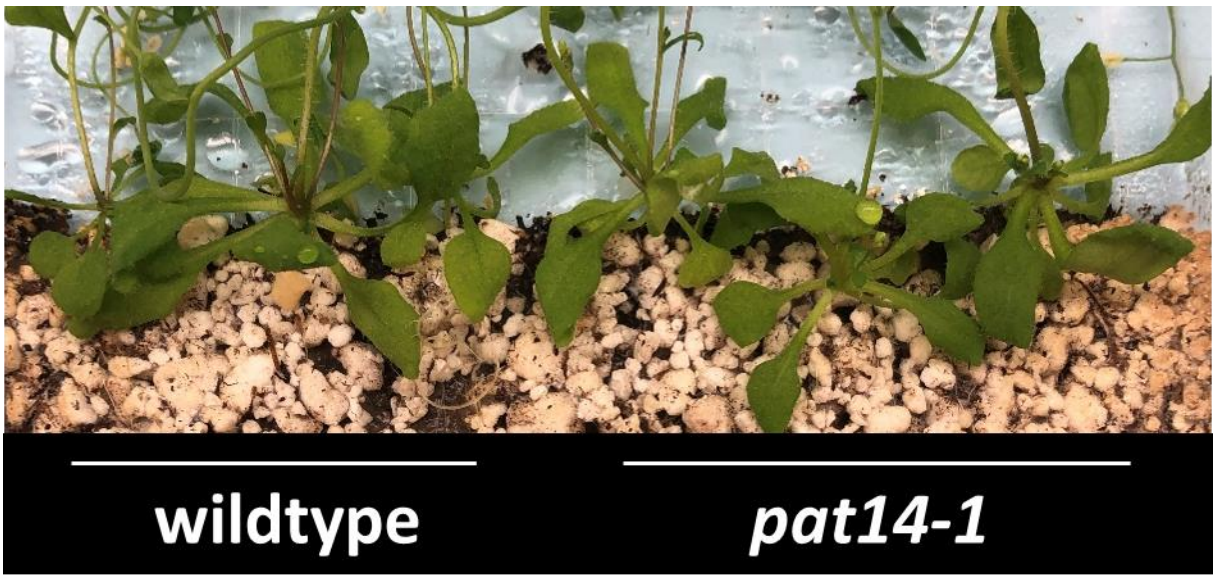

Figure 3. Plant growth on peat/perlite in plates. Arabidopsis plants were grown for 4 weeks under aseptic conditions on agar plates containing peat/perlite (1:1) and 0.45 mg/mL MiracleGro solidified with Phytoblend.

pat14-1 plants grown on agar plates containing 0.5X Murashige-Skoog nutrients plus Gamborg's vitamins did not develop the typical early senescence phenotype. To test if the nutrients and vitamins found in Murashige-Skoog fertilizer are sufficient to prevent development of the *pat14-1* phenotype, both wildtype and *pat14-1* plants were grown in pots containing peat/perlite and fertilized with either MiracleGro or 0.5X Murashige-Skoog. Plants were bottom watered every 5 days and grown for 6 weeks under long day conditions before imaging, leaf analysis, and determining mass as an estimate of size.

As expected, MiracleGro-fertilized *pat14-1* plants appeared smaller and showed leaf chlorosis not seen in the wildtype (**Figure 4**). When fertilized with Murashige-Skoog, *pat14-1* plants still appeared smaller than wildtype but did not develop the chlorosis seen in *pat14-1* plants fertilized with MiracleGro.

The percent chlorotic leaf area was analyzed from images taken at 6 weeks of age (**Figures 4 & 5**). As in previous studies, wildtype plants watered with MiracleGro showed no signs of chlorosis while *pat14-1* plants were significantly different with an average of 16% chlorotic leaf area. Watering with half-strength Murashige-Skoog significantly reduced the chlorotic leaf area of *pat14-1* plants compared to *pat14-1* plants watered with MiracleGro (**Figure 5**). In addition, Murashige-Skoog fertilized *pat14-1* plants were not significantly more chlorotic than wildtype plants at 6 weeks.

pat14-1 plants fertilized with MiracleGro weighed on average about ~60% less than wildtype plants (**Figure 6**). When fertilized with Murashige-Skoog plus Gamborg's vitamins, *pat14-1* plant weight was not significantly different from *pat14-1* plants fertilized with MiracleGro and was no longer different from wildtype plants. The average weight of Murashige-Skoog fertilized wildtype plants was intermediate between MiracleGro fertilized wildtype plants

and Murashige-Skoog fertilized *pat14-1* plants and was not significantly different from either of them. Notably, the difference between weights o the wildtype plants trended towards significance (**Table 3**). The average weight values suffer from large error bars and low *n* numbers in some conditions, which likely contributes to the inconsistencies seen in the significance tests. As a result, the effect of Murashige-Skoog fertilization on plant weight could not be determined with certainty.

It thus appears that Murashige-Skoog fertilizer is able to rescue the early senescence phenotype of *pat14-1* but not the diminished size phenotype. Further, Murashige-Skoog may negatively affect the growth of wildtype plants, but this experiment must be replicated to provide larger *n* numbers and smaller error bars.

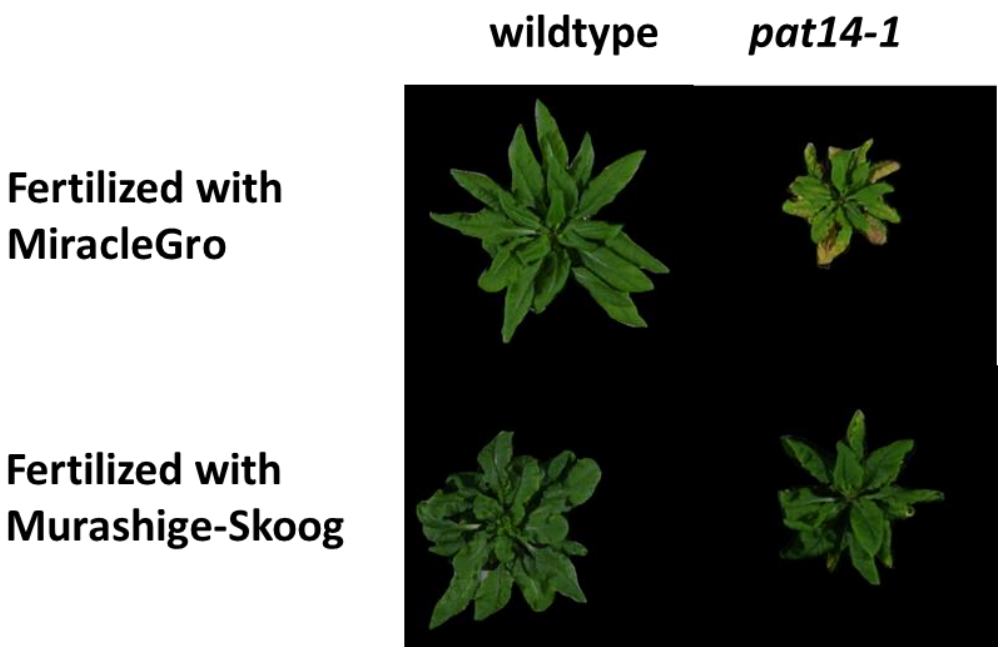

Figure 4. Size of plants grown in pots with different fertilizers. Representative images of wildtype and *pat14-1* plants grown for 6 weeks in peat/perlite. Plants were fertilized with either MiracleGro or 0.5X Murashige-Skoog plus Gamborg's vitamins.

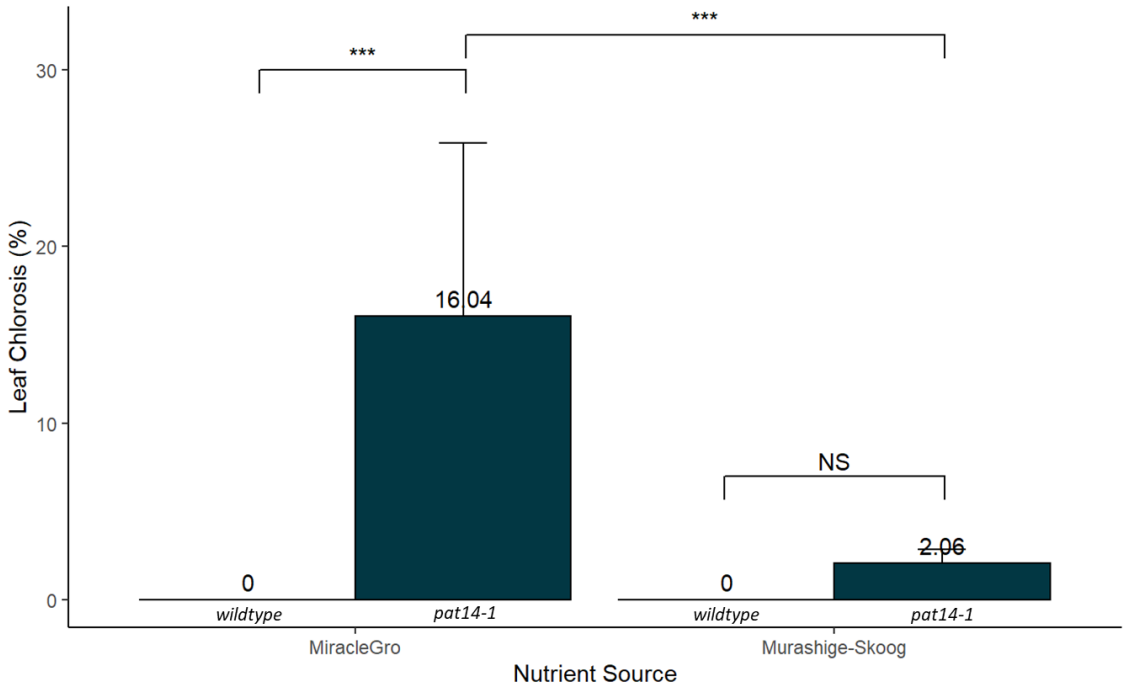

Figure 5. Chlorosis in plants grown in pots with different fertilizers. Wildtype and *pat14-1* plants were grown for 6-weeks in pots with peat/perlite and fertilized with MiracleGro or Murashige-Skoog. Values are the average leaf chlorosis area with standard deviation. *** denotes a p-value (Tukey's HSD test) less than 0.001. NS denotes a non-significant p-value. *n* = 3-7 per condition.

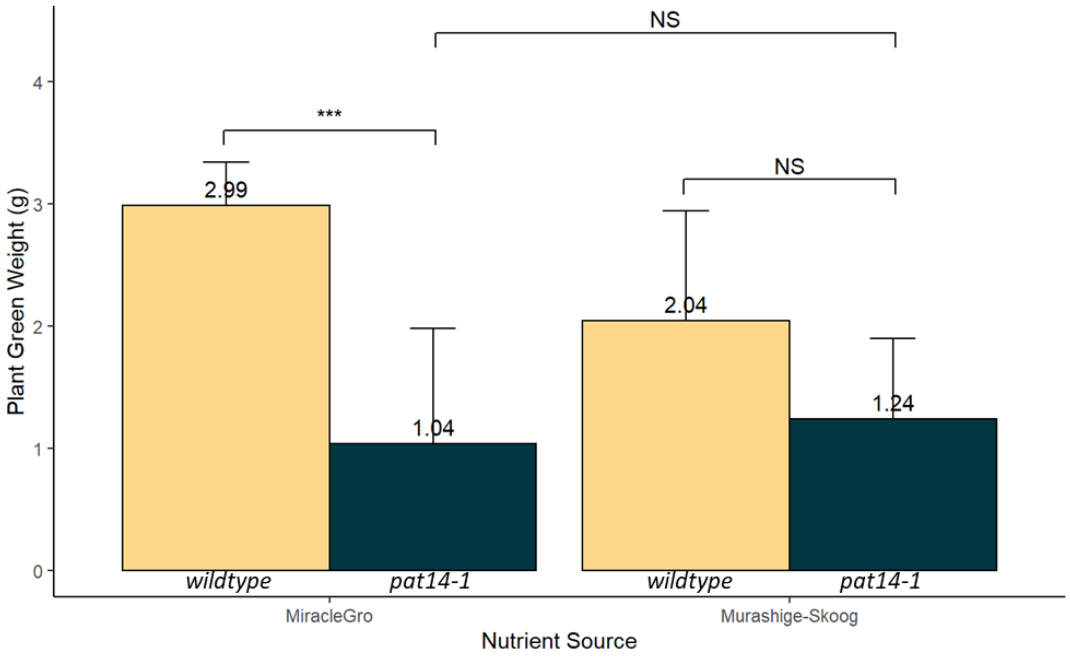

Figure 6. Weight of plants treated with different fertilizers. Wildtype and *pat14-1* plants were grown for 6 weeks in pots containing peat/perlite. Values are the average weight with standard deviation. *** denotes p-value (Tukey's HSD test) less than 0.001, ** denotes a p-value (Tukey's HSD test) less than 0.01. NS denotes a not-significant p-value. *n* = 3-7 per condition.

Table 3. *p*-values associated with weight treated with different fertilizers. Values apply to the data in **Figure 6**. Calculated with Tukey's HSD test.

Genotype 1	Nutrient Source 1	Genotype 2	Nutrient Source 2	*p*-value
wildtype	MiracleGro	*pat14-1*	MiracleGro	0.00012
wildtype	MiracleGro	wildtype	Murashige-Skoog	0.20428
pat14-1	MiracleGro	*pat14-1*	Murashige-Skoog	0.99939
wildtype	Murashige-Skoog	*pat14-1*	Murashige-Skoog	0.44994

Role of Microbiome Presence in *pat14-1* Phenotype

pat14-1 plants are smaller than wildtype and develop an early senescence phenotype when grown in pots containing peat/perlite fertilized with MiracleGro. The *pat14-1* mutant did not develop the typical senescence phenotype when grown on plates containing peat/perlite/MiracleGro under aseptic conditions (**Figure 3**). One difference between these two growth conditions is the lack of microbes in the plate growth environment. *pat14-1* plants have elevated expression of pathogen-defense and salicylic acid (SA) biosynthesis genes and so might be hypersensitive to microbes[68,73]. SA is a significant signaling molecule of senescence and pathogen response, inducing its own biosynthesis and upregulatory expression of pathogen response genes[73]. Exogenous application of SA is also capable of inducing of early senescence[73].

An unavoidable shortcoming of the previous experiment where peat/perlite was mixed with agar and poured into plates is that it does not mimic the growth medium architecture of peat/perlite in a pot or include the regular application of water and plant food. In this experiment, the peat/perlite mixture was autoclaved in plastic Magenta boxes to kill any microbes and then moistened with an autoclaved MiracleGro solution. Arabidopsis seeds were surface sterilized to remove any surface microbes before sowing in the Magenta boxes. Plants were watered once a week with autoclaved MiracleGro using aseptic technique.

The plants struggled to grow in this environment and did not achieve the size normally seen in pot-grown plants (**Figure 7**). Due to the diminished size, pixel-based methods (ImageJ) of measuring chlorosis were impossible. In addition, ImageJ often failed to distinguish plant coloration from the perlite in the peat/perlite mixture. The fresh weight of the leaf rosette (flower

stalk included) was measured. On average, *pat14-1* plants weighed only ~30% of their wildtype counterparts (**Figure 8**), similar to the ratio seen in peat/perlite grown pots. As in the previous experiment, absence of microbes did not appear to be a determining factor in the development of the *pat14-1* phenotype.

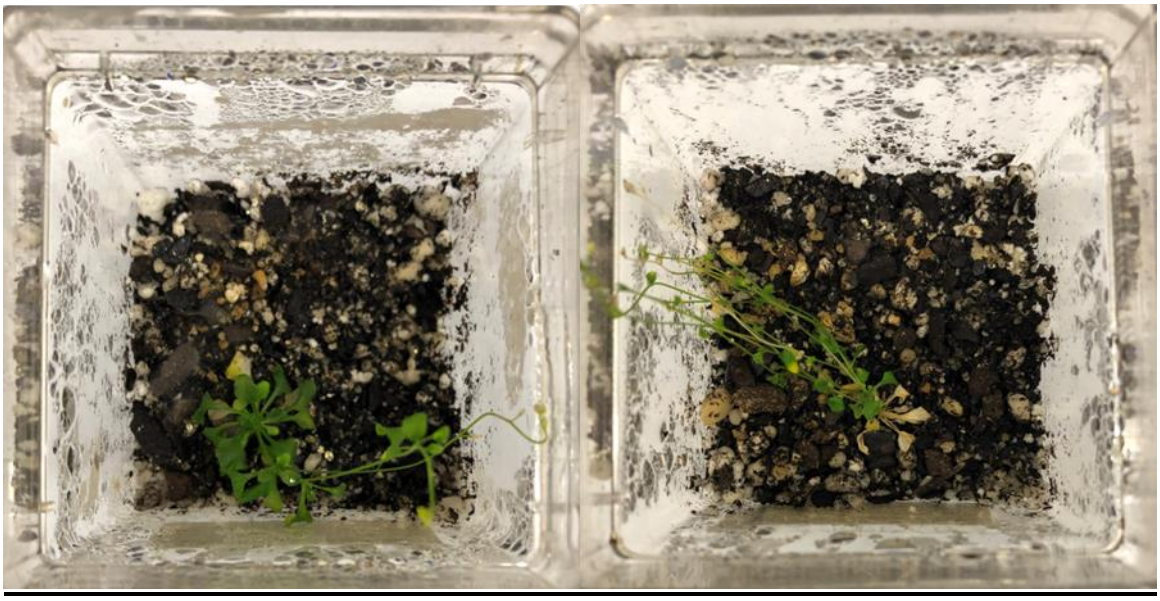

Figure 7. Growth of plants under aseptic conditions. Wildtype (left) and *pat14-1* (right) Arabidopsis plants were grown in Magenta cubes containing sterilized peat/perlite moistened with MiracleGro fertilizer under aseptic conditions for 6 weeks. The photos were taken from above looking down into the Magenta box with the lid removed.

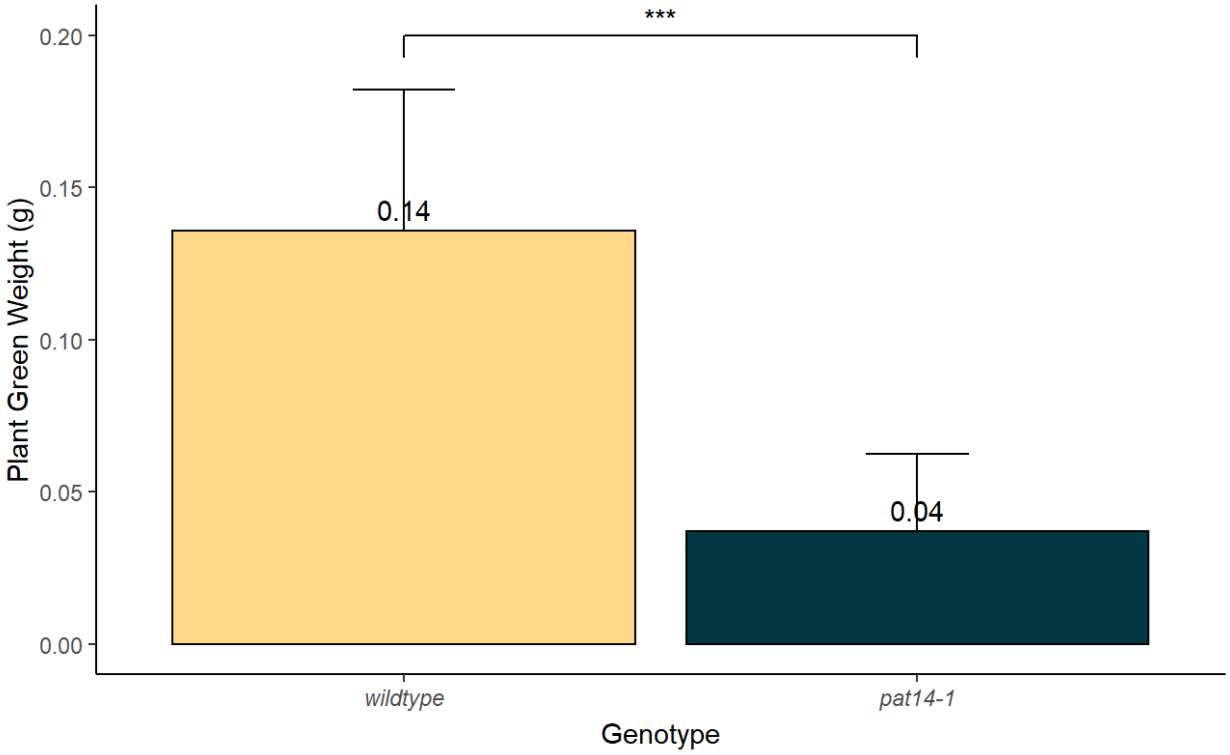

Figure 8. Weight of plants grown in Magenta cubes. Values are average weight with standard deviation. *** denotes p-value less than 0.001 calculated with Tukey's HSD test. *n* = 7 for each genotype.

Bioinformatic Approach to Predict *pat14-1* Targets

Previous work to predict PAT14 palmitoylation targets used entries from the Leaf Senescence Database, a curated collection of senescence associated genes, filtered through CSS-PALM 4.0 to identify putative palmitoylation sites and selected the top six highest scores for testing[53,62,74]. Because PAT14 is expressed throughout the Arabidopsis life cycle, not just during late development stages when senescence occurs, and because early senescence is associated with biotic and environmental stress, it seems possible that the *pat14* early senescence phenotype may be triggered by stress due to side effects of the *pat14* mutation[62]. Therefore, limiting potential PAT targets to those in the Leaf Senescence Database could constrain the search for potential targets. Here, we employed a bioinformatic script that made as few assumptions as possible, ignoring any prior association with senescence, and used the latest iteration of the palmitoylation prediction program, GPS-PALM[52]. Ideal matches would have known mutant phenotypes with similarities to the *pat14-1* phenotype.

A script was written to filter the latest Arabidopsis proteome release for predicted palmitoylated proteins using GPS-PALM and then rank those filtered proteins based on the similarity of their Gene Ontology (GO) terms with the GO terms associated with PAT14 (**Table 4**). GO terms consist of three classifications: Cellular Component, Molecular Function, and Biological Process.

Table 4. GO terms associated with PAT14. Collected from TAIR.

Accession	Name
GO:1900055	regulation of leaf senescence
GO:0018230	peptidyl-L-cysteine S-palmitoylation
GO:2000377	regulation of reactive oxygen species metabolic process
GO:0010150	leaf senescence
GO:0006612	protein targeting to membrane

Beginning with 27,655 proteins of the proteome from The Arabidopsis Information Resource, GPS-PALM narrowed the pool to 5,356 predicted palmitoylated targets[70]. These proteins were then ranked by decreasing GO term similarity to PAT14 (At3g60800). The location of the protein, as noted by Cellular Component, was ignored as PAT14 resides in the trans-Golgi body where proteins are modified before passing through to a final destination, meaning PAT14's location is unlikely to be the final location of its substrates. Molecular Function GO terms were also omitted because PAT14's Molecular Function terms relate to its acyltransferase activity and its substrates are not expected to be acyltransferases. This left us with Biological Process terms that represent the biological systems and pathways the protein is associated with.

The top two results shared five GO terms with PAT14, At1g64650 and At4g30996. Literature reviews were conducted on these two proteins for any known interactions or information. At1g64650 is Golgi S-Adenosyl Methione Transporter 1 (GoSAMT1), a S-adenosyl methionine transporter protein for polysaccharide methylation, while At4g30996 is Na^+- AND K^+-Sensitive 1 (NSK1), an endomembrane-localized scaffolding protein that supports homogalacturonan synthesis[75,76]. GoSAMT1 and NSK1 are both involved in homogalacturonan synthesis in the Golgi that is critical for plant cell wall structure and stability. Both proteins localize to the Golgi body. *gosamt1* plants have a stunted phenotype like *pat14-1* but also display shorter inflorescence stems and smaller flowers[76].

After completing the analysis, we concluded that GO term-based methods have a critical flaw when applied to the Arabidopsis PAT family of enzymes for two critical reasons. First, all 24 proteins in the PAT family share at minimum ~30% of their Biological Process terms (**Table**

5). Second, PAT proteins have very little GO term coverage. Twenty of the 24 PATs have only two Biological Process terms, while PAT14 has slightly more with 6. Due to the high similarity between PAT GO terms, the same list of possible substrates would likely be generated for any of the PAT enzymes.

Table 5. GO terms associated with Arabidopsis PATs

PAT	Total GO terms	Biological Process GO terms
PAT1	14	2
PAT2	14	2
PAT3	16	2
PAT4	18	3
PAT5	15	2
PAT6	14	2
PAT7	16	2
PAT8	16	2
PAT9	14	2
PAT10	18	4
PAT11	14	2
PAT12	14	2
PAT13	16	2
PAT14	26	6
PAT15	16	2
PAT16	14	2
PAT17	16	2
PAT18	16	2
PAT19	14	2
PAT20	16	2
PAT21	18	4
PAT22	16	2
PAT23	15	2
PAT24	22	2

Effect of Uric Acid on *pat14-1* Phenotype

The literature was evaluated to identify genes with early senescence phenotypes that might be PAT14 palmitoylation targets. This search uncovered the proteins Xanthine Dehydrogenase 1 (XDH1) and Xanthine Dehydrogenase 2 (XDH2), a pair of enzymes that degrade purines and produce uric acid to scavenge reactive oxygen species[77]. In purine degradation, XDH1 and XDH2 can either reduce NAD^+ to NADH or reduce O_2 to O_2^-, meaning that these enzymes can either scavenge reactive oxygen species or produce them[78]. XDH1 and XDH2 share 93% amino acid identity but show differences in their expression patterns. Both genes are constitutively expressed, however XDH1 is responsive to conditions such as drought, cold, and natural senescence [79].

RNAi was used to lower levels of all XDH transcripts (both *XDH1* and *XDH2*) with concomitant reduction in activity [80]. RNAi of XDH results in early senescence and a diminished size phenotype. Nakagawa et al. found that supplementing Murashige-Skoog with 100 µM uric acid rescued the diminished size phenotype of *XDH* RNAi plants[80]. Nakagawa et al. used half strength Murashige-Skoog as nutrient source whereas we fertilize pot-grown plants with MiracleGro. If PAT14 palmitoylates XDH, then I hypothesized that supplementing growth medium with uric acid should rescue the *pat14-1* phenotype in a similar way.

To test if uric acid supplementation could rescue the *pat14-1* phenotype, wildtype and *pat14-1* plants were watered with either MiracleGro or Murashige-Skoog, as well as MiracleGro or Murashige-Skoog supplemented with 100 µM uric acid. Plants were bottom watered every 5

days and grown for 6 weeks under long day conditions before imaging and quantitation of chlorosis and shoot mass.

As usual, when fertilized with MiracleGro, *pat14-1* plants appeared smaller than wildtype and showed yellowing of the leaves, indicative of early senescence (**Figure 9**). When MiracleGro fertilizer was supplemented with uric acid, wildtype and *pat14-1* grew to a more similar size and showed similar amounts of leaf yellowing. Similarly, when the fertilizer is changed from MiracleGro to half-strength Murashige-Skoog, wildtype and *pat14-1* were closer in size and showed similar levels of chlorosis. Murashige-Skoog appeared to both prevent the development of *pat14-1* early senescence and promote growth. Uric acid supplementation appeared to prevent early senescence development but did not promote plant growth.

The leaf area (%) of the plants that was chlorotic was analyzed from images (**Figure 10**). At 6 weeks of age, wildtype Arabidopsis plants watered with MiracleGro had yet to show signs of chlorosis, as expected. In contrast, *pat14-1* plants watered with MiracleGro showed an average of 16% chlorotic leaf area. When MiracleGro was supplemented with 100 µM uric acid, *pat14-1* chlorosis dropped to 2-4% of the plant and was no longer statistically different from the wildtype. *pat14-1* chlorosis was also significantly less when plants were watered with Murashige-Skoog with or without uric acid supplementation (**Figure 10**). A list of Tukey's HSD test calculated p-values for chlorosis is in **Table 6**. Across all conditions, wildtype plants did not significantly differ in the percent chlorotic area. These results showed that uric acid supplementation did ameliorate the early senescence phenotype of the *pat14-1* mutant grown in peat/perlite and fertilized with MiracleGro, indicating a possible biological connection between XDH and PAT14.

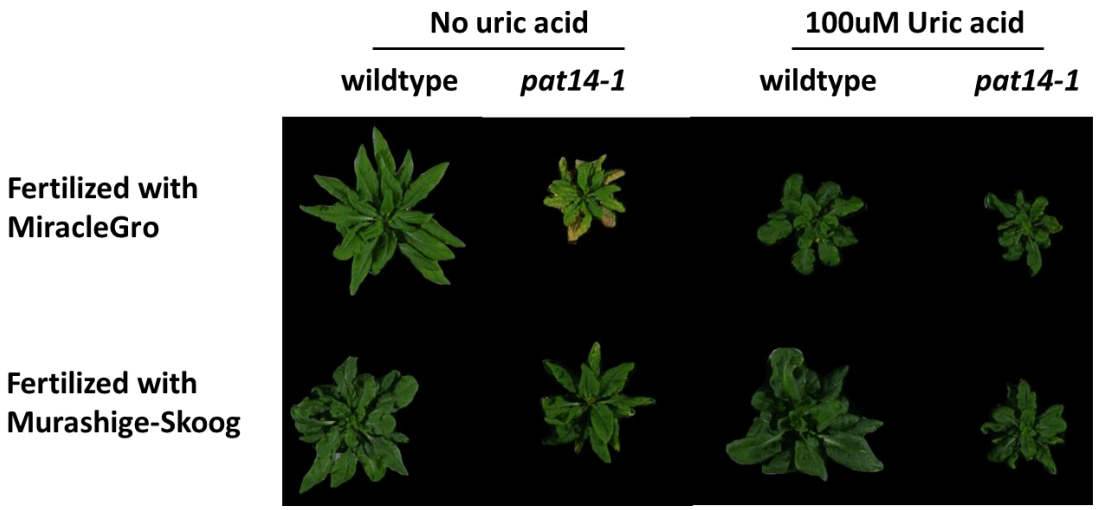

Figure 9. Plant growth with uric acid supplementation. Representative images of wildtype and *pat14-1* plants grown for 6 weeks in peat/perlite with different nutrient sources. For some plants, fertilizer was supplemented with 100 µM uric acid.

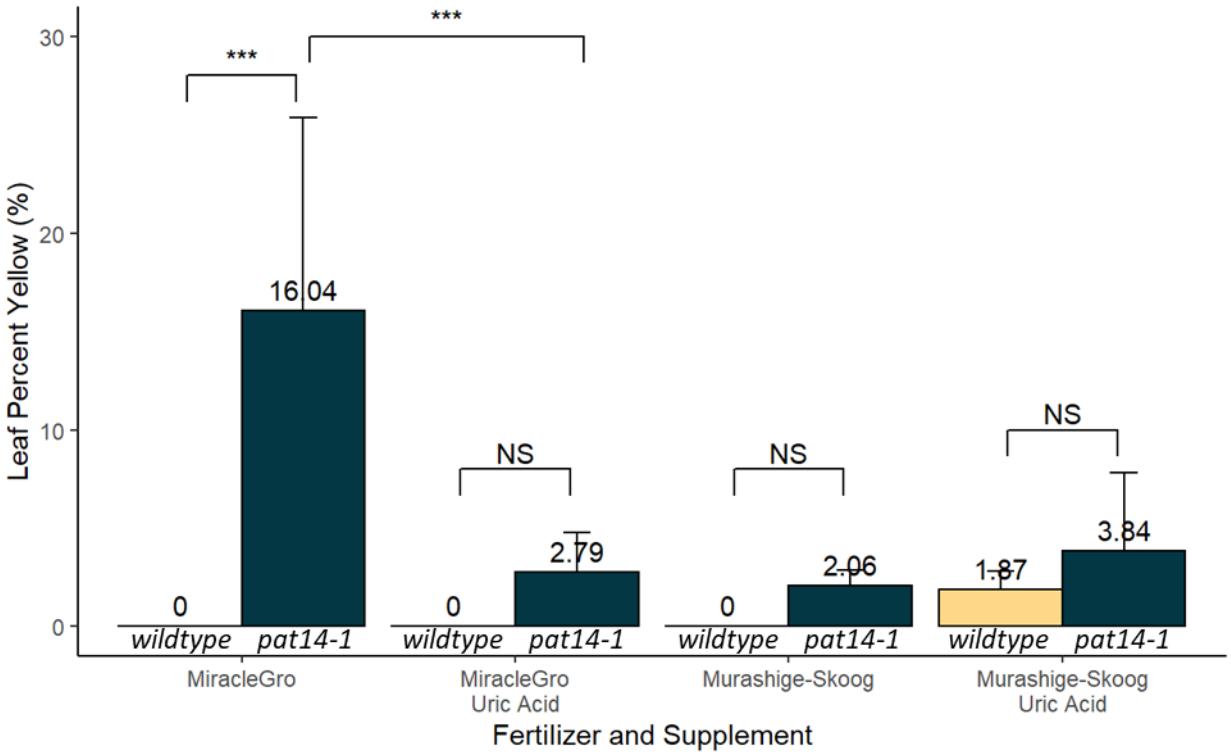

Figure 10. Plant chlorosis when fertilizer was supplemented with uric acid. Wildtype and *pat14-1* plants were grown for 6 weeks in peat/perlite. Fertilizer was either MiracleGro or Murishige-Skoog plus Gamborg's vitamins. In some cases, fertilizer was supplemented with 100 µM uric acid. Values are the average chlorotic area of the leaf with standard deviation. *** denotes a p-value (Tukey's HSD test) less than 0.001. NS denotes a not significant p-value. *n* = 3-7 per condition.

Table 6. *p*-values associated with chlorosis. Values apply to data in **Figure 10**. Calculated via Tukey's HSD test.

Genotype 1	Nutrient Source 1	Genotype 2	Nutrient Source 2	*p* -value
wildtype	MiracleGro	*pat14-1*	MiracleGro	0.00000
wildtype	MiracleGro	wildtype	MiracleGro + UA	1.00000
wildtype	MiracleGro	wildtype	Murashige-Skoog	1.00000
wildtype	MiracleGro	wildtype	Murashige-Skoog + UA	0.98957
pat14-1	MiracleGro	*pat14-1*	MiracleGro + UA	0.00008
pat14-1	MiracleGro	*pat14-1*	Murashige-Skoog	0.00003
pat14-1	MiracleGro	*pat14-1*	Murashige-Skoog + UA	0.00007
wildtype	MiracleGro + UA	*pat14-1*	MiracleGro + UA	0.97186
wildtype	MiracleGro + UA	wildtype	Murashige-Skoog	1.00000
wildtype	MiracleGro + UA	wildtype	Murashige-Skoog + UA	0.99601
pat14-1	MiracleGro + UA	*pat14-1*	Murashige-Skoog	0.99999
pat14-1	MiracleGro + UA	*pat14-1*	Murashige-Skoog + UA	0.99986
wildtype	Murashige-Skoog	*pat14-1*	Murashige-Skoog	0.99105
wildtype	Murashige-Skoog	wildtype	Murashige-Skoog + UA	0.99177
pat14-1	Murashige-Skoog	*pat14-1*	Murashige-Skoog + UA	0.99558
wildtype	Murashige-Skoog + UA	*pat14-1*	Murashige-Skoog + UA	0.98586

Supplementing fertilizer with uric acid had an effect on plant size. In comparison among wildtype plants, supplementation of MiracleGro with uric acid caused a significant size reduction in wildtype plants (**Figure 11A**) that was not reported in Nakagawa et al[80]. Fertilizing with Murashige-Skoog, either with or without uric acid did not significantly reduce the size of wildtype plants although there was a trend toward size reduction. A comparison among *pat14-1* plants showed no statistically significant differences in plant weights regardless of nutrient source or uric acid supplementation, although there was an indication that supplementation of MiracleGro with uric acid could be detrimental to growth (**Figure 11B and Table 7**). A list of Tukey's HSD test calculated p-values for plant weight is provided in **Table 7**.

When weights of wildtype and *pat14-1* plants were compared, only plants fertilized with MiracleGro showed significant weight differences (**Figure 12**). Statistically, all other comparisons of wildtype and *pat14-1* weights were not significantly different under the same conditions. This may well be due to the low *n* numbers and large error bars.

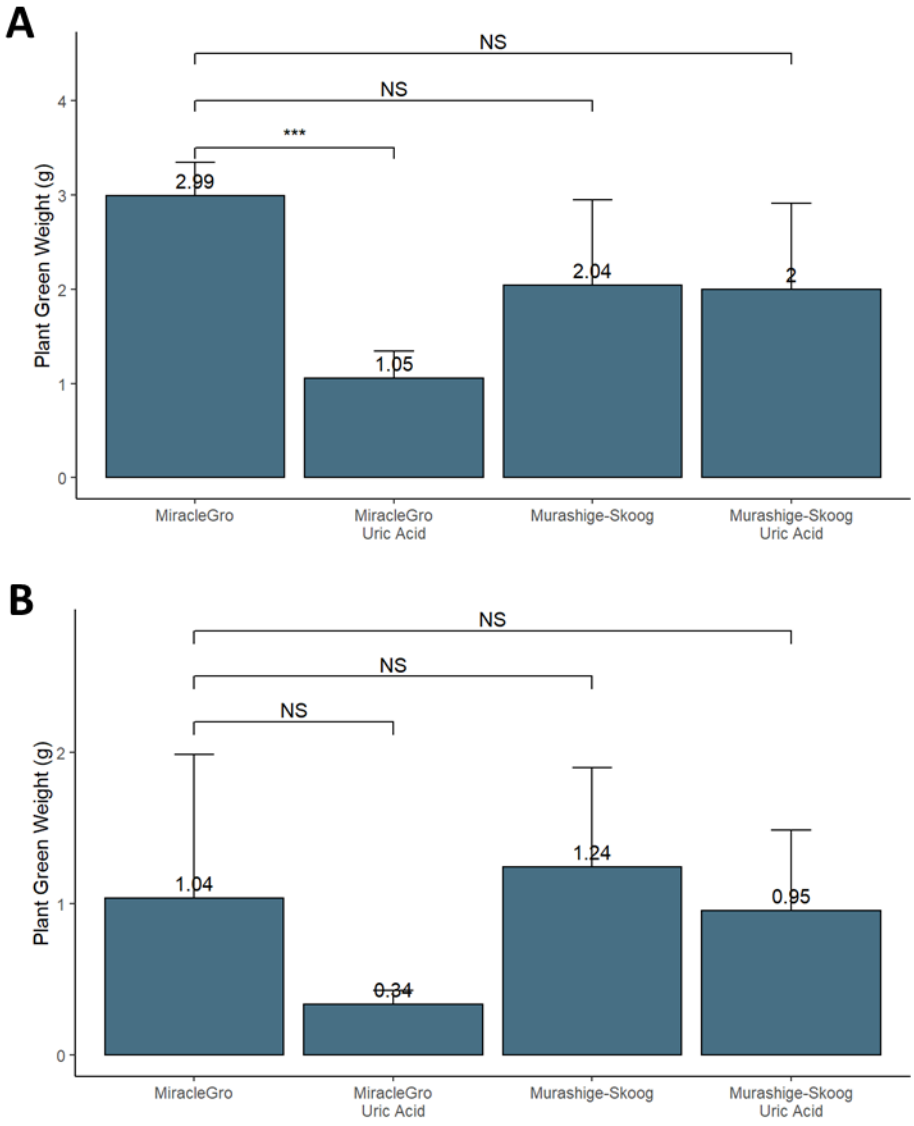

Figure 11. Weight of plants when fertilizer was supplemented with uric acid. **A**) Wildtype and **B**) *pat14-1* plants were grown for 6 weeks in peat/perlite. Fertilizer was either MiracleGro or Murishige-Skoog plus Gamborg's vitamins. In some cases, fertilizer was supplemented with 100 µM uric acid. Values are average weight with standard deviation. *** indicates a p-value (Tukey's HSD test) less than 0.001. NS indicates a non-significant p-value (Tukey's HSD test). *n* = 3-7 per condition.

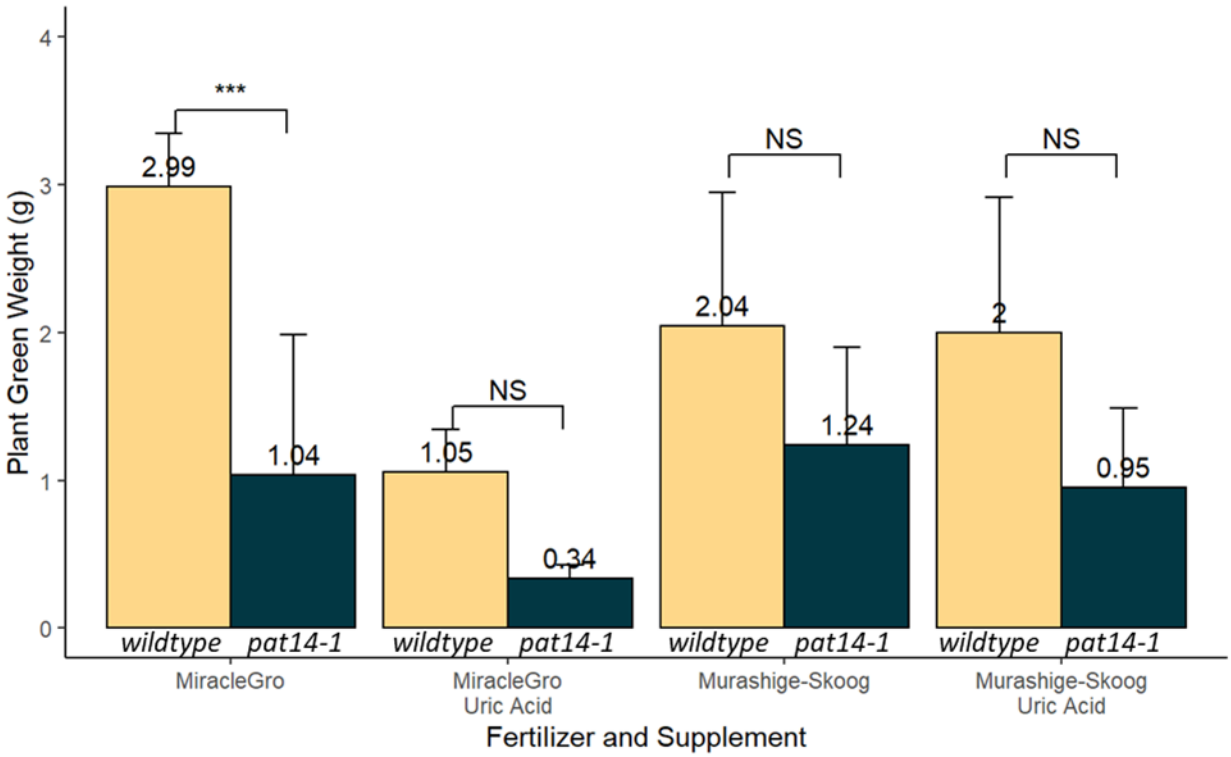

Figure 12. Weight of plants when fertilizer was supplemented with uric acid. Wildtype and *pat14-1* plants were grown for 6 weeks in peat/perlite. Fertilizer was either MiracleGro or Murishige-Skoog plus Gamborg's vitamins. In some cases, fertilizer was supplemented with 100 µM uric acid. Values are the average weight with standard deviation. *** denotes p-value (Tukey's HSD test) less than 0.001. NS denotes a non-significant p-value. *n* = 3-7 per condition.

Table 7. *p*-values associated with plant weight. Values apply to data in **Figure 12**. Calculated via Tukey's HSD test.

Genotype 1	Nutrient Source 1	Genotype 2	Nutrient Source 2	*p*-value
wildtype	MiracleGro	*pat14-1*	MiracleGro	0.00012
wildtype	MiracleGro	wildtype	MiracleGro + UA	0.00058
wildtype	MiracleGro	wildtype	Murashige-Skoog	0.20428
wildtype	MiracleGro	wildtype	Murashige-Skoog + UA	0.16026
pat14-1	MiracleGro	*pat14-1*	MiracleGro + UA	0.74519
pat14-1	MiracleGro	*pat14-1*	Murashige-Skoog	0.99939
pat14-1	MiracleGro	*pat14-1*	Murashige-Skoog + UA	1.00000
wildtype	MiracleGro + UA	*pat14-1*	MiracleGro + UA	0.78264
wildtype	MiracleGro + UA	wildtype	Murashige-Skoog	0.25477
wildtype	MiracleGro + UA	wildtype	Murashige-Skoog + UA	0.30936
pat14-1	MiracleGro + UA	*pat14-1*	Murashige-Skoog	0.48316
pat14-1	MiracleGro + UA	*pat14-1*	Murashige-Skoog + UA	0.84429
wildtype	Murashige-Skoog	*pat14-1*	Murashige-Skoog	0.44994
wildtype	Murashige-Skoog	wildtype	Murashige-Skoog + UA	1.00000
pat14-1	Murashige-Skoog	*pat14-1*	Murashige-Skoog + UA	0.99499
pat14-1	Murashige-Skoog	*wildtype*	Murashige-Skoog + UA	0.12091

Effect of PAT14 on Subcellular Localization and Expression of Xanthine Dehydrogenase

Palmitoylation drives cytosolic proteins to become permanently membrane associated, a process that can be reversed by acyl protein thioesterase. XDH1 and XDH2 are both predicted to be palmitoylated based on GPS-PALM and mass-spectrometry experiments[54]. XDH1 is shown to localize to both the cytosol and the tonoplast in a 2:1 ratio when the transgene is expressed under a 35S promoter[54,81]. To determine if PAT14 palmitoylation activity is responsible for XDH1 membrane localization, equal proportions of soluble protein and membrane protein extracts from 6-week-old plants were separated by SDS-PAGE and transferred to a PVDF membrane. The sequence of the peptide used to produce the anti-XDH1 antibody is 80% homologous with the sequence of XDH2, meaning the anti-XDH1 antibody could also cross-react with XDH2. The membrane was initially probed for XDH1, then stripped and reprobed for VM23, a vacuolar membrane marker that should only appear in the membrane protein fraction. VM23 acts as a control for correct fractionation of the plant extract.

In wildtype plants, XDH1 predominantly localized to the soluble fraction with a smaller but distinct portion in the membrane-associated fraction (**Figure 13A)**. In *pat14-1* soluble protein extracts, more XDH1 was present as compared to wildtype soluble protein extracts. In both wildtype and *pat14-1*, there was much more XDH1 in the soluble fraction than in the membrane faction, clearly exceeding the 2:1 ratio reported by Ma et al.[81]. This may be due to the fact that Ma et al. expressed XDH1 from the strong, constitutive 35S promoter while these experiments detected endogenous levels of XDH1. The XDH1 signal in the membrane-associated fraction of *pat14-1* is of similar intensity to the membrane-associated fraction of wildtype plants. Protein signal for VM23 entirely localized to the membrane associated fraction

in both wildtype and *pat14-1* as expected, indicating a clean separation of soluble and membrane protein (**Figure 13B**). Even though the gels show evidence of over-loading, because soluble and membrane samples were proportionately loaded, two preliminary conclusions can be drawn from these experiments. First, because there appeared to be no difference in the amount of XDH1 in the membrane fraction from either wildtype or *pat14-1* plants, PAT14 appears not to be the PAT that palmitoylates XDH1 or alternatively is not the only PAT that palmitoylates XDH1. Second, the higher amounts of XDH1 in the soluble fraction of *pat14-1* plants compared to wildtype plants may indicate that XDH1 could be an enzyme that is upregulated in the *pat14-1* genetic background.

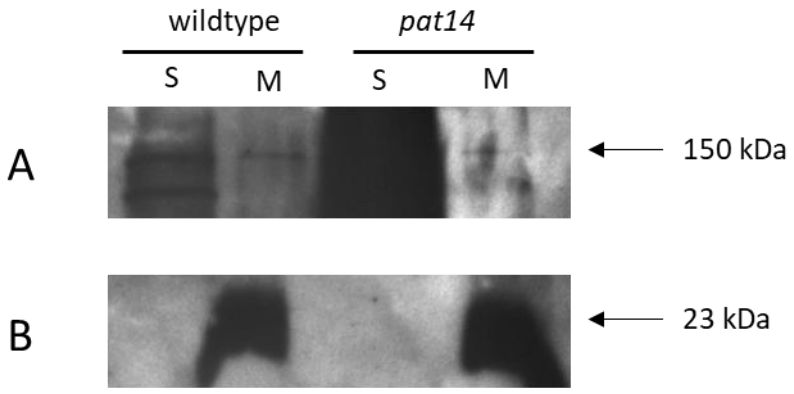

Figure 13. Immunoblot analysis of soluble and membrane protein extracts. A) anti-XDH1 and B) anti-VM23. S= soluble protein fraction; M=membrane protein fraction.

DISCUSSION

Effect of Growth Medium and Microbes on *pat14-1* Phenotype

Previous work in the Hrabak lab has shown that *pat14-1* plants grown on agar plates with Murashige-Skoog with Gamborg's vitamins as fertilizer do not show the early senescence phenotype seen when plants are grown in a non-sterile environment in peat/perlite pots with MiracleGro fertilizer. Conditions in an agar plate are, of course, different from the open-air peat/perlite conditions, so determining the phenotype-inducing condition(s) is challenging.

To begin, agar plates were cast that contained peat/perlite and MiracleGro to test if the presence of these components in plates led to the development of the same *pat14-1* early senescence phenotype as is observed in pots. The lack of *pat14-1* phenotype development indicated that the peat/perlite and MiracleGro, under these conditions, were not responsible for *pat14-1* early senescence (**Figure 4**).

Next, to evaluate if the *pat14-1* early senescence phenotype is the result of a lack of a particular nutrient or nutrients (or an overabundance of a particular nutrient(s)), plants grown in peat/perlite in pots were watered with either MiracleGro or half-strength Murashige-Skoog with Gamborg's vitamins. Similar to previous reports, *pat14-1* plants grew to about one third the size of wildtype plants when watered with MiracleGro and showed extensive leaf yellowing not seen in the wildtype. Changing the fertilizer from MiracleGro to Murashige-Skoog rescued the *pat14-1* early senescence phenotype but the effect on the reduced size phenotype was inconclusive.

Statistically, wildtype and *pat14-1* plants watered with Murashige-Skoog were not significantly different in weight and this was unexpected because the weights of *pat14-1* and wildtype plants were different when the fertilizer was MiracleGro (**Figure 12** and **Table 6**). This effect seems to be due to a decrease in the weight of wildtype plants fertilized with Murashige-Skoog nutrients, rather than a change in the weight of *pat14-1* plants. However, these results may be influenced by small sample sizes, as the wildtype weight is also not significantly different from MiracleGro-watered wildtype plant weight. Overall, the results could be strengthened by repeating the experiment with a larger number of plants per treatment. If the early senescence and reduced size phenotypes of *pat14-1* are caused by the nutrients present in MiracleGro or absent from MiracleGro, it will be difficult to pursue this further because, although the exact composition of Murashige-Skoog plus Gamborg's vitamins is known (**Table 8**), MiracleGro is a proprietary formulation. If the *pat14-1* phenotype is the result of a nutrient problem, it may be necessary to test custom formulations of Murashige-Skoog in order to control changing variables.

Table 8. Composition of Murashige-Skoog containing Gamborg's vitamins. Composition was obtained from the manufacturer (Caisson Labs).

Components	**mg/L**
Ammonium Nitrate	1650.00
Boric Acid	6.200
Calcium Chloride, Anhydrous	332.20
Cobalt Chloride, Hexhydrate	0.025
Cupric Sulfate, Pentahydrate	0.025
EDTA, Disodium, Dihydrate	37.26
Ferrous Sulfate, Heptahydrate	27.80
Magnesium Sulfate, Anhydrous	180.70
Manganese Sulfate, Monohydrate	16.900
Molybdic Acid Sodium Salt, Dihydrate	0.250
Myo-inositol	100.00
Niacin/Nicotinic Acid	1.00
Potassium Iodide	0.830
Potassium Nitrate	1900.00
Potassium Phosphate, Monobasis, Anhydrous	170.00
Pyridoxine, Hydrochloride	1.00
Thiamine, Hydrochloride	10.00
Zinc Sulfate, Heptahydrate	8.600

In addition to nutrient composition, the environmental conditions are drastically different on a plate vs. in pots. In pots, the growth medium is loose, allowing for easier growth and water is delivered at regular intervals as opposed to plates where the moisture supply from the agar is continuous. Hydroponics may be an option that allows control of nutrients without the presence of peat, perlite, or agar.

In addition to the early senescence phenotype and accompanying expression of senescence associated genes, *pat14-1* upregulates pathogen-defense genes and SA biosynthesis genes. To test whether the upregulation of pathogen-defense and SA biosynthesis genes in *pat14-1* is due to hypersensitivity to an otherwise harmless plant microbe present in non-sterile environments, wildtype and *pat14-1* seeds were surface sterilized, sown on sterilized peat/perlite, and grown in an aseptic environment to prevent exposure to many microbes as possible. Unfortunately, conditions inside the Magenta plastic containers had a negative effect on the growth and overall size of both wildtype and *pat14-1* plants. Despite the reduced size and poor condition of all of the plants, the ratio of the wildtype plant size to *pat14-1* plant sizes (3:1) was consistent with plants grown in non-aseptic conditions in pots (**Figure 5**). The diminished size of all plants in this experiment made quantifying the extent of leaf senescence difficult due to color similarity between the plants and the perlite, however by visual inspection, it appeared that *pat14-1* plants showed more chlorosis than wildtype plants. The development of both the early senescence and diminished size phenotypes under aseptic conditions indicated that the presence of microbes is unlikely to cause the phenotype in the peat/perlite conditions. Thus, it is possible that the increased SA levels, a major signal in both plant pathogen-defense and senescence, in *pat14-1* plants are not a response to a pathogen or microbe. It is more likely that the pathogen-

defense genes and SA induction is a symptom of the loss of regulation of another, currently unknown upstream process.

It is possible that peat or perlite or MiracleGro actually have a negative effect on *pat14-1* plants grown in plates even though no effect was detected. Perhaps the Phytoblend used to solidify the peat/perlite plates plays a protective role by chelating or binding harmful components from the peat, perlite, or MiracleGro.

GO Terms are Not Currently an Effective Method of Identifying PAT14 Targets

Previous work on PAT14 palmitoylation has used palmitoylation prediction programs to identify putative protein targets using entries from the Leaf Senescence Database (LSD) and filtering them for the top scoring hits with mixed results[62]. This pipeline design has two notable drawbacks. Firstly, although *pat14* mutant plants have an early senescence phenotype as they age, it does not necessarily follow that the enzymatic target of PAT14 is a senescence associated protein. It's possible that dysfunction in PAT14 substrate palmitoylation occurs far upstream of downstream pro-senescence signal cascades. Second, palmitoylation identification programs suffer from poor accuracy compared to generation of experimental data about PAT targets. In some cases, palmitoylation programs only predicted half the number of proteins identified in lab-based experiments as palmitoylated[54]. Thus, both stages of the pipeline have potentially significant gaps in coverage of possible PAT14 substrates.

In an attempt to overcome these limitations, I employed a bioinformatic script written to filter the latest Arabidopsis proteome release for predicted palmitoylated proteins and to rank them based on their GO term similarity to PAT14. By beginning with all possible proteins in the

Arabidopsis proteome, the script makes as few assumptions about the target protein as possible and emphasizes the idea that similarity in GO term sets is commonly acknowledged as being indicative of interaction (i.e., two proteins with similar GO terms are more likely to interact than two randomly selected proteins).

Unfortunately, GO term-based methods appear to have little efficacy when applied to the Arabidopsis PAT family of enzymes for two critical reasons. First, the 24 proteins in the PAT family all share ~30% of their Biological Process GO terms (**Table 4**). Most PATs, 20 out of 24, have 2 BP terms while PAT14 has the most with 6, only four of which are unique. Due to the high similarity between the enzymes' GO terms, a ranked list of possible substrates could be associated with any of the PAT enzymes, making determinations of what enzyme palmitoylates what substrate impossible. Second, Arabidopsis PAT proteins have very little GO term coverage when compared to historically well studied proteins or even to human PATs that have on average 7 more annotations than Arabidopsis PATs (**Tables 4** and **8**).

In summary, there is currently no way to differentiate between individual PATs at the current level of annotation in Arabidopsis. However, two of the top hits produced by the pipeline used here are involved in homogalacturonan synthesis and both proteins localize to the Golgi. The fact that the top two results appear to be related contradicts the conclusion that our pipeline would be expected to output nearly arbitrary matches. Even though the dwarf phenotype of *nsk1* appears different from the *pat14-1* phenotype, further investigation of these two proteins as possible PAT14 targets is warranted.

Table 9. Human PATs and their GO terms.

ZDHHC	Total GO terms	Biological Process GO terms
ZDHHC1	42	5
ZDHHC2	69	28
ZDHHC3	38	14
ZDHHC4	22	2
ZDHHC5	33	9
ZDHHC6	33	9
ZDHHC7	49	19
ZDHHC8	27	8
ZDHHC9	34	6
ZDHHC11	24	5
ZDHHC12	29	9
ZDHHC13	30	5
ZDHHC14	21	4
ZDHHC15	100	17
ZDHHC16	30	13
ZDHHC17	98	14
ZDHHC18	20	5
ZDHHC19	22	3
ZDHHC20	36	5
ZDHHC21	54	18
ZDHHC22	40	6
ZDHHC23	20	4
ZDHHC24	32	2

Xanthine Dehydrogenase 1 as a Palmitoylation Target of PAT14

Previous work on XDH1 has shown it to be palmitoylated and distributed between the cytosol and tonoplast membrane in a 2:1 ratio when expressed under a constitutive 35S promoter[54,81]. XDH1 has been shown to be upregulated under drought conditions, senescence, pathogen infection, and purine catabolism[82–85].

To determine the localization of XDH1, separate fractions containing cytosolic or membrane proteins from 6-week-old wildtype or *pat14-1* Arabidopsis plants were used for immunodetection. XDH1 was detected in both the cytosolic and membrane fractions but not in the 2:1 ratio report by Nakagawa et al[80]. Nakagawa et al. used transgenic plants over-expressing XDH1, which could affect protein distribution. Thus, it is likely that the cytosolic:membrane ratio of XDH1 reported here is representative of the true expression and distribution patterns of the XDH1 enzyme.

The amount of palmitoylated XDH1 in the membrane fraction of *pat14-1* plants appeared to be comparable to the amount in wildtype membranes (**Figure 13**), as samples were proportionally loaded and could be directly compared. This result indicated that if PAT14 palmitoylates XDH1, it is not solely responsible for the XDH1 palmitoylation. It is possible that another PAT, perhaps the closely-related PAT13, also palmitoylates XDH1 as PAT13 and PAT14 share very high sequence similarity and have additive knockout phenotypes.

More XDH1 in the cytosolic fraction was expected than in the membrane fraction, but an unexpected result from this research was the finding that the amount of XDH1 signal in the

pat14-1 soluble fraction was much greater than in the corresponding wildtype plant sample, indicating that *pat14-1* contained more XDH1 than normal. This increase may result from XDH1 induction by the WRKY75 transcription factor. WRKY75 binds W-boxes, three of which are located upstream of XDH1, and operates in a tripartite positive amplification loop with SA and H_2O_2 that starts during and promotes leaf senescence[81,86,87]. Alternatively, PAT14 might regulate ubiquitination of XDH1, preventing breakdown of XDH1. Interestingly, despite the higher concentration of cytosolic XDH1 in *pat14-1*, there was no obvious increase in putatively palmitoylated and membrane associated XDH1, indicating a possible cap on the allowable quantity of membrane associated XDH1.

XDH1's substrate specificity is cell dependent[81]. In mesophyll cells, XDH1 predominantly acts on hypoxanthine and xanthine to produce uric acid that scavenges reactive oxygen species produced in the chloroplast. In contrast, in epidermal cells, XDH1 produces superoxide (O_2^-) from NADH and O_2 in response to pathogen invasion. O_2^- can be converted to the less harmful but still damaging H_2O_2, which dramatically increased in *pat14-1*. Early senescence observed in *xdh* mutants can be rescued by supplementation with 100 µM uric acid[80]. By supplementing the fertilizer given to wildtype and *pat14-1* plants with 100 µM uric acid, I showed that this concentration of uric acid can rescue the *pat14-1* knockout, indicating that the *pat14-1* early senescence phenotype could be driven by the increased levels of H_2O_2.

The protective effect of uric acid on *pat14-1* plants raises the question of why *pat14-1* cells appeared to express more XDH1. Cells could express XDH1 to produce uric acid to counter the high levels of H_2O_2 in the *pat14-1* mutant. Alternatively, XDH1 could be producing O_2^-, which uric acid supplementation would counter. Future experiments should include protein analysis of XDH1 content in the presence of uric acid to determine if XDH1 expression

decreases when uric acid is provided or increases to produce more O_2^-. Supplementing fertilizer with uric acid might also deplete H_2O_2 levels produced from a source unrelated to XDH1. That uric acid supplementation rescues the *pat14-1* phenotype might be the result of blocking the H_2O_2 signal from causing further pro-senescence signals.

Although there were indications of a negative effect of uric acid on growth of wildtype and *pat14-1* plants, no definitive conclusion was reached due to small sample size and high variability in the data.

As mentioned previously, it's likely that PAT14 palmitoylates multiple substrates. Since the diminished size phenotype of *pat14-1* precedes development of the early senescence phenotype, PAT14 is already affecting the growth and development of Arabidopsis before visible signs of senescence appear. Uric acid supplementation was not enough to rescue the diminished size of *pat14-1* (**Figure 9**), which hints at probable pleiotropic effects of a *pat14* mutation affecting multiple proteins and pathways.

Future Directions

First, uric acid supplementation experiments must be repeated, as some of the results reported here are contradictory to published work.

Second, definitive evidence for PAT14 palmitoylation of XDH1 has yet to be demonstrated. It is possible that PAT13, with 66% sequence identity and an additive senescence phenotype when combined with a PAT14 mutant, might target the same protein substrates as PAT14. The continued presence of palmitoylated XDH1 in *pat14-1* plants could be attributed to

PAT13 activity. This could be tested by measuring XDH1 levels in the membrane fractions of other PAT mutants, such as *pat13,* and the double mutants *pat13pat14*.

Third, XDH1 converts its substrate, either NADH or xanthine, to NAD^+/O_2^- or uric acid, respectively[81]. Measuring the levels of xanthine in *pat14-1* plants would provide insights into the biochemical pathways upstream of XDH1 in the absence of PAT14 activity.

Fourth, determining the amount of XDH1 in *pat14-1* plants when uric acid is supplemented could determine which biochemical mechanism activity XDH1 is performing under these conditions. When uric acid is provided to the plant, cells no longer need to express XDH1 to produce their own supply uric acid. If XDH1 protein levels drop when uric acid is provided, this could indicate that XDH1 was expressed to produce uric acid. Alternatively, if XDH1 is expressed to produce more O_2^-, XDH1 levels would increase further when uric acid is provided to produce more O_2.

List of References

(1) Ramazi, S.; Zahiri, J. Post-Translational Modifications in Proteins: Resources, Tools and Prediction Methods. *Database* **2021**. https://doi.org/10.1093/DATABASE/BAAB012.

(2) Nadolski, M. J.; Linder, M. E. Protein Lipidation. *FEBS J* **2007**, *274* (20), 5202–5210. https://doi.org/10.1111/J.1742-4658.2007.06056.X.

(3) Roth, A. F.; Feng, Y.; Chen, L.; Davis, N. G. The Yeast DHHC Cysteine-Rich Domain Protein Akr1p Is a Palmitoyl Transferase. *J. Cell Bio.* **2002**, *159* (1), 23–28. https://doi.org/10.1083/jcb.200206120.

(4) Chang, C. C. Y.; Sun, J.; Chang, T.-Y. Membrane-Bound O-Acyltransferases (MBOATs). *Front. Biol* **2011**, *6* (3), 177–182. https://doi.org/10.1007/s11515-011-1149-z.

(5) Resh, M. D. Covalent Lipid Modifications of Proteins. *Curr Biol* **2013**, *23* (10), R431–R435. https://doi.org/10.1016/J.CUB.2013.04.024.

(6) Camp, L. A.; Hofmann, S. L.; Tang, W.-J. The Purification and Properties of a Palmitoyl-Protein Thioesterase That Cleaves Palmitate From H-Ras. *J Biol Chem* **1993**, *268* (30), 22566–22574. https://doi.org/10.1016/S0021-9258(18)41567-0.

(7) Lin, D. T. S.; Conibear, E. Enzymatic Protein Depalmitoylation by Acyl Protein Thioesterases. *Biochem Soc Trans* **2015**, *43*, 193–198. https://doi.org/10.1042/BST20140235.

(8) Young, F. B.; Butland, S. L.; Sanders, S. S.; Sutton, L. M.; Hayden, M. R. Putting Proteins in Their Place: Palmitoylation in Huntington Disease and Other Neuropsychiatric Diseases. *Prog Neurobiol* **2012**, *97* (2), 220–238. https://doi.org/10.1016/J.PNEUROBIO.2011.11.002.

(9) Nishimura, A.; Linder, M. E. Identification of a Novel Prenyl and Palmitoyl Modification at the CaaX Motif of Cdc42 That Regulates RhoGDI Binding. *Mol Cell Biol* **2013**, *33* (7), 1417. https://doi.org/10.1128/MCB.01398-12.

(10) Jang, D.; Kwon, H.; Jeong, K.; Lee, J.; Pak, Y. Essential Role of Flotillin-1 Palmitoylation in the Intracellular Localization and Signaling Function of IGF-1 Receptor. *J Cell Sci* **2015**, *128* (11), 2179–2190. https://doi.org/10.1242/JCS.169409.

(11) Yurchak, L. K.; Sefton, B. M. Palmitoylation of Either Cys-3 or Cys-5 Is Required for the Biological Activity of the Lck Tyrosine Protein Kinase. *Mol Cell Biol* **1995**, *15* (12), 6914–6922. https://doi.org/10.1128/MCB.15.12.6914.

(12) Tanimura, N.; Saitoh, S. I.; Kawano, S.; Kosugi, A.; Miyake, K. Palmitoylation of LAT Contributes to Its Subcellular Localization and Stability. *Biochem Biophys Res Commun* **2006**, *341* (4), 1177–1183. https://doi.org/10.1016/J.BBRC.2006.01.076.

(13) Guardiola-Serrano, F.; Rossin, A.; Cahuzac, N.; Lückerath, K.; Melzer, I.; Mailfert, S.; Marguet, D.; Zö Rnig, M.; Hueber, A. O. Palmitoylation of Human FasL Modulates Its Cell Death-Inducing Function. *Cell Death Dis* **2010**, *1* (10), e88. https://doi.org/10.1038/CDDIS.2010.62.

(14) Taruno, A.; Sun, H.; Nakajo, K.; Murakami, T.; Ohsaki, Y.; Kido, M. A.; Ono, F.; Marunaka, Y. Post-translational Palmitoylation Controls the Voltage Gating and Lipid Raft Association of the CALHM1 Channel. *J Physiol* **2017**, *595* (18), 6121–6145. https://doi.org/10.1113/JP274164.

(15) Dowen, R. H.; Engel, J. L.; Shao, F.; Ecker, J. R.; Dixon, J. E. A Family of Bacterial Cysteine Protease Type III Effectors Utilizes Acylation-Dependent and -Independent Strategies to Localize to Plasma Membranes. *J. Biol. Chem.* **2009**, *284* (23), 15867–15879. https://doi.org/10.1074/JBC.M900519200.

(16) Shahinian, S.; Silvius, J. R. Doubly-Lipid-Modified Protein Sequence Motifs Exhibit Long-Lived Anchorage to Lipid Bilayer Membranes1. *Biochemistry* **1995**, *34*, 3813–3822.

(17) Batistič, O. Genomics and Localization of the Arabidopsis DHHC-Cysteine-Rich Domain s-Acyltransferase Protein Family. *Plant Physiol* **2012**, *160* (3), 1597–1612. https://doi.org/10.1104/pp.112.203968.

(18) Wang, W.; Yuan, T.; Qian, M.; Yan, F.; Yang, L.; He, Q.; Yang, B.; Lu, J.; Zhu, H. Post-Translational Modification of KRAS: Potential Targets for Cancer Therapy. *Acta Pharmacol Sin* **2021**, *42* (8), 1201–1211. https://doi.org/10.1038/S41401-020-00542-Y.

(19) Ohno, Y.; Kihara, A.; Sano, T.; Igarashi, Y. Intracellular Localization and Tissue-Specific Distribution of Human and Yeast DHHC Cysteine-Rich Domain-Containing Proteins. *Biochimica et Biophysica Acta (BBA) - Molecular and Cell Biology of Lipids* **2006**, *1761* (4), 474–483. https://doi.org/10.1016/J.BBALIP.2006.03.010.

(20) Frénal, K.; Tay, C. L.; Mueller, C.; Bushell, E. S.; Jia, Y.; Graindorge, A.; Billker, O.; Rayner, J. C.; Soldati-Favre, D. Global Analysis of Apicomplexan Protein S-Acyl Transferases Reveals an Enzyme Essential for Invasion. *Traffic* **2013**, *14* (8), 895–911. https://doi.org/10.1111/TRA.12081.

(21) Jennings, B. C.; Linder, M. E. DHHC Protein S-Acyltransferases Use Similar Ping-Pong Kinetic Mechanisms but Display Different Acyl-CoA Specificities. *J Biol Chem* **2012**, *287* (10), 7236–7245. https://doi.org/10.1074/JBC.M111.337246.

(22) Stix, R.; Lee, C. J.; Faraldo-Gómez, J. D.; Banerjee, A. Structure and Mechanism of DHHC Protein Acyltransferases. *J Mol Biol* **2020**, *432* (18), 4983–4998. https://doi.org/10.1016/j.jmb.2020.05.023.

(23) Mitchell, D. A.; Mitchell, G.; Ling, Y.; Budde, C.; Deschenes, R. J. Mutational Analysis of Saccharomyces Cerevisiae Erf2 Reveals a Two-Step Reaction Mechanism for Protein Palmitoylation by DHHC Enzymes. *J Biol Chem* **2010**, *285* (49), 38104–38114. https://doi.org/10.1074/JBC.M110.169102.

(24) Blanc, M.; David, F.; Abrami, L.; Migliozzi, D.; Armand, F.; Bürgi, J.; van der Goot, F. G. SwissPalm: Protein Palmitoylation Database. *F1000Res* **2015**, *4* (261). https://doi.org/10.12688/F1000RESEARCH.6464.1/DOI.

(25) Lemonidis, K.; Gorleku, O. A.; Sanchez-Perez, M. C.; Grefen, C.; Chamberlain, L. H. The Golgi S-Acylation Machinery Comprises ZDHHC Enzymes with Major Differences in Substrate Affinity and S-Acylation Activity. *Mol Biol Cell* **2014**, *25* (24), 3870–3883. https://doi.org/10.1091/mbc.E14-06-1169.

(26) Montoro, A. G.; Ramirez, S. C.; Taubas, J. V. The Canonical DHHC Motif Is Not Absolutely Required for the Activity of the Yeast S-Acyltransferases Swf1 and Pfa4. *J. Biol. Chem.* **2015**, *290* (37), 22448–22459. https://doi.org/10.1074/JBC.M115.651356.

(27) Fukata, Y.; Fukata, M. Protein Palmitoylation in Neuronal Development and Synaptic Plasticity. *Nat Rev Neurosci* **2010**, *11* (3), 161–175. https://doi.org/10.1038/NRN2788.

(28) Malgapo, M. I. P.; Linder, M. E. Substrate Recruitment by ZDHHC Protein Acyltransferases. *Open Biol* **2021**, *11* (4). https://doi.org/10.1098/RSOB.210026.

(29) Thomas, G. M.; Hayashi, T.; Chiu, S. L.; Chen, C. M.; Huganir, R. L. Palmitoylation by DHHC5/8 Targets GRIP1 to Dendritic Endosomes to Regulate AMPA-R Trafficking. *Neuron* **2012**, *73* (3), 482–496. https://doi.org/10.1016/J.NEURON.2011.11.021.

(30) Thomas, G. M.; Hayashi, T.; Huganir, R. L.; Linden, D. J. DHHC8-Dependent PICK1 Palmitoylation Is Required for Induction of Cerebellar Long-Term Synaptic Depression. *J Neurosci* **2013**, *33* (39), 15401–15407. https://doi.org/10.1523/JNEUROSCI.1283-13.2013.

(31) Sanders, S. S.; Hernandez, L. M.; Soh, H.; Karnam, S.; Walikonis, R. S.; Tzingounis, A. v.; Thomas, G. M. The Palmitoyl Acyltransferase ZDHHC14 Controls Kv1-Family Potassium Channel Clustering at the Axon Initial Segment. *Elife* **2020**, *9*, 1–32. https://doi.org/10.7554/ELIFE.56058.

(32) Salaun, C.; Greaves, J.; Chamberlain, L. H. The Intracellular Dynamic of Protein Palmitoylation. *J. Cell Biol.* **2010**, *191* (7), 1229–1238. https://doi.org/10.1083/jcb.201008160.

(33) Greaves, J.; Prescott, G. R.; Gorleku, O. A.; Chamberlain, L. H. Regulation of SNAP-25 Trafficking and Function by Palmitoylation. *Biochem Soc Trans.* 2010, pp 163–166. https://doi.org/10.1042/BST0380163.

(34) Levental, I.; Grzybek, M.; Simons, K. Greasing Their Way: Lipid Modifications Determine Protein Association with Membrane Rafts. *Biochemistry* **2010**, *49* (30), 6305–6316. https://doi.org/10.1021/BI100882Y.

(35) Rocks, O.; Peyker, A.; Kahms, M.; Verveer, P. J.; Koerner, C.; Lumbierres, M.; Kuhlmann, J.; Waldmann, H.; Wittinghofer, A.; Bastiaens, P. I. H. An Acylation Cycle Regulates Localization and Activity of Palmitoylated Ras Isoforms. *Science* **2005**, *307* (5716), 1746–1752. https://doi.org/10.1126/SCIENCE.1105654.

(36) Olson, M. F.; Marais, R. Ras Protein Signalling. *Semin Immunol* **2000**, *12* (1), 63–73. https://doi.org/10.1006/SMIM.2000.0208.

(37) Zhao, L.; Lobo, S.; Dong, X.; Ault, A. D.; Deschenes, R. J. Erf4p and Erf2p Form an Endoplasmic Reticulum-Associated Complex Involved in the Plasma Membrane Localization of Yeast Ras Proteins. *J Biol Chem* **2002**, *277* (51), 49352–49359. https://doi.org/10.1074/JBC.M209760200.

(38) Swarthout, J. T.; Lobo, S.; Farh, L.; Croke, M. R.; Greentree, W. K.; Deschenes, R. J.; Linder, M. E. DHHC9 and GCP16 Constitute a Human Protein Fatty Acyltransferase with Specificity for H- and N-Ras. *J Biol Chem* **2005**, *280* (35), 31141–31148. https://doi.org/10.1074/JBC.M504113200.

(39) Goodwin, J. S.; Drake, K. R.; Rogers, C.; Wright, L.; Lippincott-Schwartz, J.; Philips, M. R.; Kenworthy, A. K. Depalmitoylated Ras Traffics to and from the Golgi Complex via a Nonvesicular Pathway. *J. Cell Bio.* **2005**, *170* (2), 261–272. https://doi.org/10.1083/JCB.200502063.

(40) Ponimaskin, E.; Dityateva, G.; Ruonala, M. O.; Fukata, M.; Fukata, Y.; Kobe, F.; Wouters, F. S.; Delling, M.; Bredt, D. S.; Schachner, M.; Dityatev, A. Fibroblast Growth Factor-Regulated Palmitoylation of the Neural Cell Adhesion Molecule Determines Neuronal Morphogenesis. *J Neurosci* **2008**, *28* (36), 8897–8907. https://doi.org/10.1523/JNEUROSCI.2171-08.2008.

(41) Zhang, W.; Trible, R. P.; Samelson, L. E. LAT Palmitoylation: Its Essential Role in Membrane Microdomain Targeting and Tyrosine Phosphorylation during T Cell Activation. *Immunity* **1998**, *9* (2), 239–246. https://doi.org/10.1016/S1074-7613(00)80606-8.

(42) Zeppelin, T.; Pedersen, K. B.; Berglund, N. A.; Periole, X.; Schiøtt, B. Effect of Palmitoylation on the Dimer Formation of the Human Dopamine Transporter. *Sci. Rep.* **2021**, *11* (1), 1–15. https://doi.org/10.1038/s41598-021-83374-y.

(43) Singaraja, R. R.; Kang, M. H.; Vaid, K.; Sanders, S. S.; Vilas, G. L.; Arstikaitis, P.; Coutinho, J.; Drisdel, R. C.; el Din El-Husseini, A.; Green, W. N.; Berthiaume, L.;

Hayden, M. R. Palmitoylation of ATP-Binding Cassette Transporter A1 Is Essential for Its Trafficking and Function. *Circ Res* **2009**, *105* (2), 138–147. https://doi.org/10.1161/CIRCRESAHA.108.193011.

(44) Zhang, Z.; Li, X.; Yang, F.; Chen, C.; Liu, P.; Ren, Y.; Sun, P.; Wang, Z.; You, Y.; Zeng, Y. X.; Li, X. DHHC9-Mediated GLUT1 S-Palmitoylation Promotes Glioblastoma Glycolysis and Tumorigenesis. *Nat. Commun.* **2021**, *12* (1), 1–12. https://doi.org/10.1038/s41467-021-26180-4.

(45) Simons, K.; Sampaio, J. L. Membrane Organization and Lipid Rafts. *Cold Spring Harb Perspect Biol* **2011**, *3* (10), 1–17. https://doi.org/10.1101/CSHPERSPECT.A004697.

(46) Gagnoux-Palacios, L.; Dans, M.; Van't Hof, W.; Mariotti, A.; Pepe, A.; Meneguzzi, G.; Resh, M. D.; Giancotti, F. G. Compartmentalization of Integrin A6β4 Signaling in Lipid Rafts. *J. Cell Biol.* **2003**, *162* (7), 1189–1196. https://doi.org/10.1083/JCB.200305006.

(47) Abrami, L.; Leppla, S. H.; Gisou Van Der Goot, F. Receptor Palmitoylation and Ubiquitination Regulate Anthrax Toxin Endocytosis. *J Cell Biol* **2006**, *172* (2), 309–320. https://doi.org/10.1083/JCB.200507067.

(48) Jochmann, R.; Holz, P.; Sticht, H.; Stürzl, M. Validation of the Reliability of Computational O-GlcNAc Prediction. *Biochim Biophys Acta* **2014**, *1844* (2), 416–421. https://doi.org/10.1016/J.BBAPAP.2013.12.002.

(49) Song, J.; Wang, H.; Wang, J.; Leier, A.; Marquez-Lago, T.; Yang, B.; Zhang, Z.; Akutsu, T.; Webb, G. I.; Daly, R. J. PhosphoPredict: A Bioinformatics Tool for Prediction of Human Kinase-Specific Phosphorylation Substrates and Sites by Integrating Heterogeneous Feature Selection. *Sci. Rep.* **2017**, *7* (1), 1–19. https://doi.org/10.1038/s41598-017-07199-4.

(50) Kumari, B.; Kumar, R.; Kumar, M. PalmPred: An SVM Based Palmitoylation Prediction Method Using Sequence Profile Information. *PLoS One* **2014**, *9* (2), e89246. https://doi.org/10.1371/JOURNAL.PONE.0089246.

(51) Shi, S. P.; Sun, X. Y.; Qiu, J. D.; Suo, S. B.; Chen, X.; Huang, S. Y.; Liang, R. P. The Prediction of Palmitoylation Site Locations Using a Multiple Feature Extraction Method. *J Mol Graph Model* **2013**, *40*, 125–130. https://doi.org/10.1016/J.JMGM.2012.12.006.

(52) Ning, W.; Jiang, P.; Guo, Y.; Wang, C.; Tan, X.; Zhang, W.; Peng, D.; Xue, Y. GPS-Palm: A Deep Learning-Based Graphic Presentation System for the Prediction of S-Palmitoylation Sites in Proteins. *Brief. Bioinformatics* **2020**, *00* (December 2019), 1–12. https://doi.org/10.1093/bib/bbaa038.

(53) Zhou, F.; Xue, Y.; Yao, X.; Xu, Y. CSS-Palm: Palmitoylation Site Prediction with a Clustering and Scoring Strategy (CSS). *Bioinformatics* **2006**, *22* (7), 894–896. https://doi.org/10.1093/BIOINFORMATICS/BTL013.

(54) Kumar, M.; Carr, P.; Turner, S. R. An Atlas of Arabidopsis Protein S-Acylation Reveals Its Widespread Role in Plant Cell Organization and Function. *Nat Plants* **2022**, *8* (6), 670–681. https://doi.org/10.1038/s41477-022-01164-4.

(55) Blanc, M.; David, F. P. A.; van der Goot, F. G. SwissPalm 2: Protein S-Palmitoylation Database. *Methods in Molecular Biology* **2019**, *2009*, 203–214. https://doi.org/10.1007/978-1-4939-9532-5_16/COVER/.

(56) Serino, G.; Marzi, D. Arabidopsis Thaliana as an Experimental Organism. *eLS* **2018**, 1–9. https://doi.org/10.1002/9780470015902.A0002031.PUB3.

(57) Mergner, J.; Frejno, M.; List, M.; Papacek, M.; Chen, X.; Chaudhary, A.; Samaras, P.; Richter, S.; Shikata, H.; Messerer, M.; Lang, D.; Altmann, S.; Cyprys, P.; Zolg, D. P.; Mathieson, T.; Bantscheff, M.; Hazarika, R. R.; Schmidt, T.; Dawid, C.; Dunkel, A.; Hofmann, T.; Sprunck, S.; Falter-Braun, P.; Johannes, F.; Mayer, K. F. X.; Jürgens, G.; Wilhelm, M.; Baumbach, J.; Grill, E.; Schneitz, K.; Schwechheimer, C.; Kuster, B. Mass-Spectrometry-Based Draft of the Arabidopsis Proteome. *Nature* **2020**, *579* (7799), 409–414. https://doi.org/10.1038/s41586-020-2094-2.

(58) Chen, D.; Hao, F.; Mu, H.; Ahsan, N.; Thelen, J. J.; Stacey, G. S-Acylation of P2K1 Mediates Extracellular ATP-Induced Immune Signaling in Arabidopsis. *Nat Commun* **2021**, *12* (1). https://doi.org/10.1038/S41467-021-22854-1.

(59) Zhou, L. Z.; Li, S.; Feng, Q. N.; Zhang, Y. L.; Zhao, X.; Zeng, Y. lun; Wang, H.; Jiang, L.; Zhang, Y. Protein S-ACYL Transferase10 Is Critical for Development and Salt Tolerance in Arabidopsis. *Plant Cell* **2013**, *25* (3), 1093–1107. https://doi.org/10.1105/TPC.112.108829.

(60) Chai, S.; Ge, F. R.; Zhang, Y.; Li, S. S-Acylation of CBL10/SCaBP8 by PAT10 Is Crucial for Its Tonoplast Association and Function in Salt Tolerance. *J Integr Plant Biol* **2020**, *62* (6), 718–722. https://doi.org/10.1111/JIPB.12864/SUPPINFO.

(61) Wan, Z. Y.; Chai, S.; Ge, F. R.; Feng, Q. N.; Zhang, Y.; Li, S. Arabidopsis PROTEIN S-ACYL TRANSFERASE4 Mediates Root Hair Growth. *Plant Journal* **2017**, *90* (2), 249–260. https://doi.org/10.1111/tpj.13484.

(62) Lai, J.; Yu, B.; Cao, Z.; Chen, Y.; Wu, Q.; Huang, J.; Yang, C. Two Homologous Protein S-Acyltransferases, PAT13 and PAT14, Cooperatively Regulate Leaf Senescence in Arabidopsis. *J Exp Bot* **2015**, *66* (20), 6345–6353. https://doi.org/10.1093/jxb/erv347.

(63) Li, Y.; Scott, R.; Doughty, J.; Grant, M.; Qi, B. Protein S-Acyltransferase 14: A Specific Role for Palmitoylation in Leaf Senescence in Arabidopsis. *Plant Physiol* **2016**, *170* (1), 415–428. https://doi.org/10.1104/pp.15.00448.

(64) Winter, D.; Vinegar, B.; Nahal, H.; Ammar, R.; Wilson, G. v.; Provart, N. J. An "Electronic Fluorescent Pictograph" Browser for Exploring and Analyzing Large-Scale Biological Data Sets. *PLoS One* **2007**, *2* (8), e718. https://doi.org/10.1371/JOURNAL.PONE.0000718.

(65) Lepine, J. The Subcellular Localization of Palmitoyltransferases in Arabidopsis Thaliana, University of New Hampshire, 2013.

(66) Alonso, J. M.; Stepanova, A. N.; Leisse, T. J.; Kim, C. J.; Chen, H.; Shinn, P.; Stevenson, D. K.; Zimmerman, J.; Barajas, P.; Cheuk, R.; Gadrinab, C.; Heller, C.; Jeske, A.; Koesema, E.; Meyers, C. C.; Parker, H.; Prednis, L.; Ansari, Y.; Choy, N.; Deen, H.; Geralt, M.; Hazari, N.; Hom, E.; Karnes, M.; Mulholland, C.; Ndubaku, R.; Schmidt, I.; Guzman, P.; Aguilar-Henonin, L.; Schmid, M.; Weigel, D.; Carter, D. E.; Marchand, T.; Risseeuw, E.; Brogden, D.; Zeko, A.; Crosby, W. L.; Berry, C. C.; Ecker, J. R. Genome-Wide Insertional Mutagenesis of Arabidopsis Thaliana. *Science* **2003**, *301* (5633), 653–657. https://doi.org/10.1126/SCIENCE.1086391.

(67) Černý, M.; Habánová, H.; Berka, M.; Luklová, M.; Brzobohatý, B. Hydrogen Peroxide: Its Role in Plant Biology and Crosstalk with Signaling Networks. *Int. J. Mol. Sci.* **2018**, *19* (9), 2812. https://doi.org/10.3390/IJMS19092812.

(68) Zhao, X. Y.; Wang, J. G.; Song, S. J.; Wang, Q.; Kang, H.; Zhang, Y.; Li, S. Precocious Leaf Senescence by Functional Loss of PROTEIN S-ACYL TRANSFERASE14 Involves the NPR1-Dependent Salicylic Acid Signaling. *Sci Rep* **2016**, *6* (September 2015), 1–15. https://doi.org/10.1038/srep20309.

(69) Cheng, C. Y.; Krishnakumar, V.; Chan, A. P.; Thibaud-Nissen, F.; Schobel, S.; Town, C. D. Araport11: A Complete Reannotation of the Arabidopsis Thaliana Reference Genome. *Plant J.* **2017**, *89* (4), 789–804. https://doi.org/10.1111/TPJ.13415.

(70) Lamesch, P.; Berardini, T. Z.; Li, D.; Swarbreck, D.; Wilks, C.; Sasidharan, R.; Muller, R.; Dreher, K.; Alexander, D. L.; Garcia-Hernandez, M.; Karthikeyan, A. S.; Lee, C. H.; Nelson, W. D.; Ploetz, L.; Singh, S.; Wensel, A.; Huala, E. The Arabidopsis Information Resource (TAIR): Improved Gene Annotation and New Tools. *Nucleic Acids Res* **2012**, *40* (D1). https://doi.org/10.1093/NAR/GKR1090.

(71) Schneider, C. A.; Rasband, W. S.; Eliceiri, K. W. NIH Image to ImageJ: 25 Years of Image Analysis. *Nat. Methods.* **2012**, *9* (7), 671–675. https://doi.org/10.1038/nmeth.2089.

(72) Kaplan, U. Phenotypic Characterization of Palmitoyltransferase Mutants of Arabidopsis Thaliana, University of New Hampshire, 2010.

(73) Peng, Y.; Yang, J.; Li, X.; Zhang, Y. Salicylic Acid: Biosynthesis and Signaling. *Annu Rev Plant Biol* **2021**, *72*, 761–791. https://doi.org/10.1146/annurev-arplant-081320-092855.

(74) Li, Z.; Zhang, Y.; Zou, D.; Zhao, Y.; Wang, H. L.; Zhang, Y.; Xia, X.; Luo, J.; Guo, H.; Zhang, Z. LSD 3.0: A Comprehensive Resource for the Leaf Senescence Research Community. *Nucleic Acids Res* **2020**, *48* (D1), D1069–D1075. https://doi.org/10.1093/nar/gkz898.

(75) Lathe, R. S.; McFarlane, H. E.; Khan, G. A.; Ebert, B.; Ramírez-Rodríguez, E. A.; Noord, N.; Bhalerao, R.; Persson, S. A DUF1068 Protein Acts as a Pectin Biosynthesis Scaffold

and Maintains Golgi Morphology and Cell Adhesion in Arabidopsis. *bioRxiv* **2021**. https://doi.org/10.1101/2021.05.03.442108.

(76) Temple, H.; Phyo, P.; Yang, W.; Lyczakowski, J. J.; Echevarría-Poza, A.; Yakunin, I.; Parra-Rojas, J. P.; Terrett, O. M.; Saez-Aguayo, S.; Dupree, R.; Orellana, A.; Hong, M.; Dupree, P. Discovery of Putative Golgi S-Adenosyl Methionine Transporters Reveals the Importance of Plant Cell Wall Polysaccharide Methylation. *bioRxiv* **2021**. https://doi.org/10.1101/2021.07.06.451061.

(77) Hille, R.; Nishino, T. Xanthine Oxidase and Xanthine Dehydrogenase. *FASEB J.* **1995**, *9* (11), 995–1003.

(78) Zarepour, M.; Kaspari, K.; Stagge, S.; Rethmeier, R.; Mendel, R. R.; Bittner, F. Xanthine Dehydrogenase AtXDH1 from Arabidopsis Thaliana Is a Potent Producer of Superoxide Anions via Its NADH Oxidase Activity. *Plant Mol Biol* **2010**, *72* (3), 301–310. https://doi.org/10.1007/s11103-009-9570-2.

(79) Hesberg, C.; Hänsch, R.; Mendel, R. R.; Bittner, F. Tandem Orientation of Duplicated Xanthine Dehydrogenase Genes from Arabidopsis Thaliana: Differential Gene Expression and Enzyme Activities. *J. Biol. Chem.* **2004**, *279* (14), 13547–13554. https://doi.org/10.1074/jbc.M312929200.

(80) Nakagawa, A.; Sakamoto, S.; Takahashi, M.; Morikawa, H.; Sakamoto, A. The RNAi-Mediated Silencing of Xanthine Dehydrogenase Impairs Growth and Fertility and Accelerates Leaf Senescence in Transgenic Arabidopsis Plants. *Plant Cell Physiol* **2007**, *48* (10), 1484–1495. https://doi.org/10.1093/pcp/pcm119.

(81) Ma, X.; Wang, W.; Bittner, F.; Schmidt, N.; Berkey, R.; Zhang, L.; King, H.; Zhang, Y.; Feng, J.; Wen, Y.; Tan, L.; Li, Y.; Zhang, Q.; Deng, Z.; Xiong, X.; Xiao, S. Dual and Opposing Roles of Xanthine Dehydrogenase in Defense-Associated Reactive Oxygen Species Metabolism in Arabidopsis. *Plant Cell* **2016**, *28* (5), 1108–1126. https://doi.org/10.1105/tpc.15.00880.

(82) Yesbergenova, Z.; Yang, G.; Oron, E.; Soffer, D.; Fluhr, R.; Sagi, M. The Plant Mo-Hydroxylases Aldehyde Oxidase and Xanthine Dehydrogenase Have Distinct Reactive Oxygen Species Signatures and Are Induced by Drought and Abscisic Acid. *The Plant Journal* **2005**, *42* (6), 862–876. https://doi.org/10.1111/J.1365-313X.2005.02422.X.

(83) Pastori, G. M.; del Río, L. A. Natural Senescence of Pea Leaves (An Activated Oxygen-Mediated Function for Peroxisomes). *Plant Physiol* **1997**, *113* (2), 411–418. https://doi.org/10.1104/PP.113.2.411.

(84) Montalbini, P. Changes in Xanthine Oxidase Activity in Bean Leaves Induced by Uromyces Phaseoli Infection. *Journal of Phytopathology* **1992**, *134* (1), 63–74. https://doi.org/10.1111/J.1439-0434.1992.TB01213.X.

(85) Montalbini, P. Effect of Rust Infection on Purine Catabolism Enzyme Levels in Wheat Leaves. *Physiol Mol Plant Pathol* **1995**, *46* (4), 275–292. https://doi.org/10.1006/PMPP.1995.1022.

(86) Guo, P.; Li, Z.; Huang, P.; Li, B.; Fang, S.; Chu, J.; Guo, H. A Tripartite Amplification Loop Involving the Transcription Factor WRKY75, Salicylic Acid, and Reactive Oxygen Species Accelerates Leaf Senescence. *Plant Cell* **2017**, *29* (11), 2854–2870. https://doi.org/10.1105/tpc.17.00438.

(87) Eulgem, T.; Somssich, I. E. Networks of WRKY Transcription Factors in Defense Signaling. *Curr Opin Plant Biol* **2007**, *10* (4), 366–371. https://doi.org/10.1016/J.PBI.2007.04.020.